DI 106995
Drs. G.H. van der KOLK
EERSTE MEDEWERKER
BCRS PROGRAMMABUREAU

USP-2
01-05

ENVISAT - Actual Evaporation

Z. Su
S. Jacobs

BCRS 01-05 MD

COMMISSIE REMOTE SENSING

Informatiecentrum
Rijkswaterstaat
Meetkundige Dienst

ENVISAT - Actual Evaporation

Z. Su
S. Jacobs

Wageningen University & Research
Centre, Alterra Green World Research

USP-2 report 01-05
USP-2 project 4.2/AP-13

ISBN 90 54 11 350 2

May 2001

This report describes a project carried out in the framework of the User Support Programme (USP-2) under responsibility of the Netherlands Remote Sensing Board (BCRS)

Abstract

This is a progress report for the project "ENVISAT - Actual Evaporation: Evaluation of algorithms to estimate actual evaporation of land surfaces with AATSR and MERIS observations", BCRS: 4.2/AP-13

The general objective of the project is to evaluate selected algorithms to estimate actual evaporation using radiances observed with imaging radiometers in the visible to thermal infrared spectral region.

In this report, we have developed the Surface Energy Balance System (SEBS) for estimation of turbulent heat fluxes for applications to high spatial resolution data. Consequently, SEBS is applied to several sites in Europe (Spain, Italy and the Netherlands) with different climates and land surface conditions.

Based on the case studies, the SEBS has been partially validated. Since the current project is limited by its available finance and time constraint (circa 15% of necessary finance), we have just focused to demonstrate the utility of SEBS for different climate and land surface conditions. No attempt has been made to refine the different procedures in order to improve the input data and consequently the model estimates.

Further effort is required to consolidate the findings in future projects.

Key-words: *remote sensing; land surface processes; actual evaporation*

Contents

Abstract ii

Contents iii

Acknowledgements v

Executive summary vii

1 Introduction 1

2 Brief Description of the Surface Energy Balance System (SEBS) for estimation of turbulent heat fluxes 3

3 Estimation of evaporation using SEBS – EFEDA 13

4 Estimation of evaporation using SEBS – Tuscany 21

5 Estimation of evaporation using SEBS - Netherlands 35

6 Conclusions and overview of future work 49

References 53

List of Acronyms and Abbreviations 57

Acknowledgements

The present phase of the project is a result of fruitful national and international scientific collaboration.

The data sets used in this study have been provided by several co-operating organisations for which we would like to extend our gratitude. The authors acknowledge all the people and institutions who have realized the several field experiments, whose data are used in this study. The advice from and discussions with Drs. G.H. van der Kolff and Dr.ir. N.J.J. Bunnik (BCRS) have been invaluable in the completion of this project.

The project is carried out by Alterra Green World Research, Wageningen, with

- Departamento de Termodinamica, Universidad de Valencia (UniValencia), Burjassot, Valencia, Spain;
- Lanzhou Institute of Plateau Atmospheric Physics, Chinese Academy of Science (LIPAP), China

as cooperating institutions.

Executive summary

This is a progress report for the project "ENVISAT - Actual Evaporation: Evaluation of algorithms to estimate actual evaporation of land surfaces with AATSR and MERIS observations", BCRS: 4.2/AP-13

The general objective of the project is to evaluate selected algorithms to estimate actual evaporation using radiances observed with imaging radiometers in the visible to thermal infrared spectral region.

In this report, the following activities and achievements are presented:

- A Brief Description of the Surface Energy Balance System (SEBS) for estimation of turbulent heat fluxes is described for applications to high spatial resolution data
- Estimation of evaporation using SEBS – EFEDA: A case study is presented using TMS data from the Barrax area, Spain.
- Estimation of evaporation using SEBS – Tuscany: A case study is conducted for a field campaign area in Italy
- Estimation of evaporation using SEBS – Netherlands: Three case studies are conducted for the Netherlands.

Based on the case studies, the SEBS has been partially validated. Since the current project is limited by its available finance and time constraint (circa 15% of necessary finance), we have just focused to demonstrate the utility of SEBS for different climate and land surface conditions. No attempt has been made to refine the different procedures in order to improve the input data and the consequently the model estimates.

Further effort is required to consolidate the findings in future projects.

1 Introduction

Land surface evaporation is a significant mechanism in land surface-atmosphere interactions. Evaporation is the largest term in the water balance of watersheds in a broad spectrum of environments and it is a measure of the allocation of net radiation at the surface and of soil water availability. Its nature depends on several land surface variables characterized by high spatial variability. Imaging radiometers provide estimates of two essential variables to assess evaporation of heterogeneous land surfaces: surface albedo and surface temperature. The former is the main determinant of net radiation and of its spatial variability, while the latter is a measure of the partition of net radiation into sensible and latent heat flux. Many efforts, as documented in literature, have been spent on developing algorithms to estimate and map actual evaporation of land surfaces using airborne and space borne imaging radiometers. Algorithms proposed vary from simple linear relationships to complex models of soil vegetation atmosphere transfer of heat and momentum (SVATs). The former aim at estimating daily evaporation using one observation of surface temperature around midday, the latter use also observations of surface albedo and estimates of other land surface variables such as aerodynamic roughness. Accuracy of estimates range from moderate to poor, but are often comparable with direct observations such as done with eddy correlation devices. The difficulty with remote sensing of actual evaporation is three-fold: 1) accuracy of observation of surface temperature and albedo; 2) accuracy of estimates of other land surface variables; 3) characterization of near surface boundary layer variables, e.g. air temperature and humidity. This problem is further compounded by spatial variability: simpler algorithms may give satisfactory results over relatively homogeneous land surfaces, while failing when dealing with rather heterogeneous cases.

The objective of the present project is to evaluate selected algorithms to estimate actual evaporation using radiances observed with imaging radiometers in the visible to thermal infrared spectral region. Due to the limited budget (around 15% of the required necessary budget) allocated to the present phase of the project, only the Surface Energy Balance System (SEBS) will be evaluated.

Chapter 2 gives a brief description of the SEBS. Chapter 3 describes application of SEBS to a data set collected in Barrax, during the EFEDA field campaign. Chapter 4 gives results for application of SEBS to a Landsat scene acquired in Tuscany, Italy. Chapter 5 presents results for applications of SEBS to three Landsat scenes in the Netherlands. Conclusions and overview of future work are summarized in Chapter 6.

2 Brief Description of the Surface Energy Balance System (SEBS) for estimation of turbulent heat fluxes

(Z. Su)

Abstract
A brief description of the Surface Energy Balance System (SEBS) is given for the estimation of atmospheric turbulent fluxes and surface evaporation using satellite earth observation data in the visible, near infra-red, and thermal infrared frequency range.

SEBS consists of the following components:
1. Preprocessing to derive land surface physical parameters, such as albedo, emissivity, temperature, vegetation coverage etc. from spectral reflectance and radiance measurements;
2. A model for the determination of the roughness length for heat transfer (Su et al. 2000);
3. The BAS (Bulk Atmospheric Similarity) theory for determination of friction velocity, sensible heat flux and the Obukhov stability length (Brutsaert, 1999)
4. The SEBI (Surface Energy Balance Index) concept for determination of evaporative fraction (Menenti & Choudhury, 1993).

In this report, SEBS will be applied to several high resolution data sets to evaluate its utility.

This part is an excerpt of the work by Su (2001) and is included in this report for easy reference when the model results are discussed. A more detailed analysis based on in-situ point measurements has been given by Su (2001).

2.1. Introduction

A brief description of the Surface Energy Balance System (SEBS) is given in this report. SEBS is developed for the estimation of atmospheric turbulent fluxes and surface evaporation using satellite earth observation data in the visible, near infra-red, and thermal infrared frequency range.

SEBS consists of the following components:

1. Preprocessing to derive land surface physical parameters, such as albedo, emissivity, temperature, vegetation coverage etc. from spectral reflectance and radiance;
2. A model for the determination of the roughness length for heat transfer (Su et al. 2000);
3. The BAS (Bulk Atmospheric Similarity) theory for determination of friction velocity, sensible heat flux and the Obukhov stability length (Brutsaert, 1999);
4. The SEBI (Surface Energy Balance Index) concept for determination of evaporative fraction (Menenti & Choudhury, 1993).

In the present set-up, SEBS requires as inputs three sets of information. The first set consists of albedo, temperature, fractional vegetation coverage and leaf area index (when

such information is not explicitly available, the Normalized Difference Vegetation Index – NDVI is used as a surrogate), and the height of the vegetation (or roughness height). These inputs can be derived from remote sensing data in conjunction with other information on the land surface. The second set includes the reference height, at which pressure, temperature, humidity, and wind speed are available. The reference height is the measurement height for point application and the height of the planetary boundary height for regional application. This data set can also be variables estimated by a large scale meteorological model. The third data set includes downward longwave radiation, and downward solar radiation which can either be direct measurements, model output or parameterization.

2.2 SEBS components

1. Determination of land surface physical parameters

Land surface parameters such as albedo, emissivity, temperature, vegetation coverage, vegetation height, leaf area index, etc. are needed in determination of the surface energy balance. Different methods have been proposed in past studies to derive these parameters based on spectral reflectance and radiance data (Verhoef, 1998; Su *et al.*, 1998, 1999; Su, 2000; Li *et al.*, 2000).

The methods used by Su *et al.* (1999) for the TMS (Thematic Mapper Simulator) data are used in this study to derive land surface parameters for TMS data and Landsat TM.

2. Components of SEBS

2.1. Surface energy balance terms

The surface energy balance is commonly written as

$$R_n = G_0 + H + \lambda E \tag{2.1}$$

Where R_n is the net radiation, G_0 is the soil heat flux, H is the turbulent sensible heat flux, and λE is the turbulent latent heat flux.

The equation to calculate the net radiation is given by

$$R_n = (1-\alpha)\cdot R_{swd} + \varepsilon \cdot R_{lwd} - \varepsilon \cdot \sigma \cdot T_0^4 \tag{2.2}$$

where α is the albedo, R_{swd} the downward solar radiation, R_{lwd} the downward long wave radiation, ε the emissivity of the surface, σ the Stefan-Bolzmann constant, and T_0 the surface temperature.

The equation to calculate soil heat flux is parameterized as

$$G_0 = R_n \cdot [\Gamma_c + (1-f_c)\cdot(\Gamma_s - \Gamma_c)] \tag{2.3}$$

in which we assume the ratio of soil heat flux to net radiation $\Gamma_c = 0.05$ for full vegetation canopy (Monteith 1973) and $\Gamma_s = 0.315$ for bare soil (Kustas and Daughtry 1989). An interpolation is then performed between these limiting cases using the fractional canopy coverage, f_c.

After computing the sensible heat flux from the bulk approach to be discussed below, and together with the net radiation and soil heat flux with Eqs. (2-2,3), the latent heat flux can be derived as an energy balance residual from (2-1) as

$$\lambda E = R_n - G_0 - H \tag{2-4}$$

2.2. A bulk approach for determination of friction velocity, sensible heat flux and the Obukhov stability length

Models of energy and mass transfer between the land surface and the atmosphere, especially those designed for numerical weather prediction or for climate studies, usually use a bulk parameterization based on Monin-Obukhov similarity (MOS) theory. In remote sensing of surface energy balance, the bulk formulation has also been the most widely used method. As pointed out recently by Brutsaert (1998), unless there is a major break through for the description of the turbulence at and near the land surface, similarity is likely to remain as the main, if not the only, practical approach for the estimation of energy and mass transfer between the land surface and the atmosphere in the near future. Other formulations based on surface bulk transfer coefficients or the various resistances and conductance parameters are in fact also based on similarity. While MOS relates surface fluxes to surface variables and variables in the atmospheric surface layer (ASL), the bulk atmospheric boundary layer (ABL) similarity (BAS) proposed by Brutsaert (1982, 1999) relates surface fluxes to surface variables and the mixed layer atmospheric variables. In order to accurately calculate the sensible heat flux by means of similarity theory, the roughness height for heat transfer must be accurately determined. We will use the model proposed by Su *et al.* (2000).

In the ASL, the similarity relationships for the profiles of the mean wind speed, u, and the mean temperature, $\theta_0 - \theta_a$, are usually written in integral form as

$$u = \frac{u_*}{k}\left[\ln\left(\frac{z-d}{z_{0m}}\right) - \Psi_m\left(\frac{z-d}{L}\right) + \Psi_m\left(\frac{z_{0m}}{L}\right)\right] \tag{2-5}$$

$$\theta_0 - \theta_a = \frac{H}{ku_*\rho C_p}\left[\ln\left(\frac{z-d}{z_{0h}}\right) - \Psi_h\left(\frac{z-d}{L}\right) + \Psi_h\left(\frac{z_{0h}}{L}\right)\right] \tag{2-6}$$

where height z is measured above the surface, $u_* = (\tau_0/\rho)^{1/2}$ is the friction velocity, τ_0 is the surface shear stress, ρ is the density of air, $k = 0.4$ is Von Karman's constant, d is the zero plane displacement height, z_{0m} is the roughness height for momentum transfer, θ_0 is the potential temperature at the surface, θ_a is the potential air temperature at height z, z_{0h} is the scalar roughness height for heat transfer, ψ_m and ψ_h are the stability correction functions for momentum and sensible heat transfer respectively, L is the Obukhov length defined as

$$L = -\frac{\rho C_p u_*^3 \theta_v}{kgH} \tag{2-7}$$

where g is the acceleration due to gravity, θ_v is the potential virtual temperature near the surface. In this study, we adopt the criteria proposed by Brutsaert (1999) to decide if the MOS or the BAS stability corrections should be used.

For field measurements performed at a height of a few meters above ground, all calculations use the MOS functions given by Brutsaert (1999). By replacing the MOS stability functions with the BAS functions proposed by Brutsaert (1999), the system of eqs. (2-5,6,7) can be used to relate surface fluxes to surface variables and the mixed layer atmospheric variables. The criterion proposed by Brutsaert (1999) is used to determine if MOS or BAS scaling is appropriate for a given situation (details to be discussed later in the text).

The sensible heat flux is obtained by solving the system of non-linear Eqs. (2-5,6,7) using the method of Broyden (Press *et al.*, 1997). It is important to note that the derivation of the sensible heat flux using eqs. (2-5,6,7) requires only the wind speed and temperature at the reference height as well as the surface temperature and is independent of other surface energy balance terms.

2.3. A model for the determination of the roughness length for heat transfer

When near surface wind speed and vegetation parameters (height and leaf area index) are available, the within-canopy turbulence model proposed by Massman (1997) can be used to estimate the aerodynamic parameters, the displacement height, d_0, and the roughness height, z_{0m}, for momentum. This model has been shown by Su et al. (2000) to produce reliable estimates of the aerodynamic parameters.

If only the height of the vegetation is available, the relationships proposed by Brutsaert (1982) may be used.

If a detailed land use classification is available, the tabulated values of Wieringa (1986, 1993) can be used. However since the aerodynamic parameters depend also on the wind speed and direction, besides the surface characteristics (e.g. Bosveld, 1999), the latter two approaches should only be used when the first method is not applicable, due to lack of data.

As an another alternative when all of the above information is not available or not convenient, the aerodynamic parameters can be related to vegetation indices derived from satellite data. However in this case, care must be taken, because the vegetation indices saturate at higher vegetation densities.

The scalar roughness height for heat transfer, z_{0h}, can be derived from

$$z_{oh} = z_{0m} / \exp\left(kB^{-1}\right) \tag{2-8}$$

where B^{-1} is the inverse of Stanton number, a dimensionless heat transfer coefficient. The model proposed by Su et al. (2000) is used to estimate kB^{-1}:

$$kB^{-1} = \frac{kC_d}{4C_t \frac{u_*}{u(h)}\left(1-e^{-n/2}\right)} f_c^2 + \frac{k \cdot {}^{u_*}\!/_{u(h)} \cdot {}^{z_{0m}}\!/_{h}}{C_t^*} f_c^2 f_s^2 + kB_s^{-1} f_s^2 \tag{2-9}$$

where f_c is the fractional canopy coverage and f_s its compliment. C_d is the drag coefficient of the foliage elements assumed to take the value of 0.2. C_t is the heat transfer coefficient of the leaf. For most canopies and environmental conditions, C_t is

bounded as $0.005N \le C_t \le 0.075N$ (N is number of sides of a leaf to participate in heat exchange), $u(h)$ is the horizontal wind speed at the canopy top. The heat transfer coefficient of the soil is given by $C_t^* = \mathrm{Pr}^{-2/3}\,\mathrm{Re}_*^{-1/2}$, where Pr is the Prandtl number (0.71, Massman 1999b) and the roughness Reynolds number $\mathrm{Re}_* = h_s u_* / \nu$, with h_s the roughness height of the soil. The kinematic viscosity of the air is given by $\nu = 1.327 \cdot 10^{-5} (p_0/p)(T/T_0)^{1.81}$ (Massman 1999b), with p and T the ambient pressure and temperature and $p_0 = 101.3$ kPa and $T_0 = 273.15$ K. For bare soil surface kB_s^{-1} is calculated according to Brutsaert (1982)

$$kB_s^{-1} = 2.46(\mathrm{Re}_*)^{1/4} - \ln[7.4] \tag{2-10}$$

According to this formulation, the three terms in the right hand side of Eq. (2-9) represent the contributions of canopy only, canopy-soil interaction and soil only, respectively. Eq. (2-9) reduces to limiting cases of canopy only for $f_c = 1$ and soil surface only for $f_s = 1$.

In this study, the within-canopy wind speed profile extinction coefficient, n, is formulated as a function of the cumulative leaf drag area at the canopy top

$$n = \frac{C_d \cdot LAI}{2u_*^2 / u(h)^2} \tag{2-11}$$

2.4. The SEBI (Surface Energy Balance Index) concept for determination of evaporative fraction

The Surface Energy Balance Index (SEBI) concept was proposed by Menenti and Choudhury (1993) on the basis of the concept of Crop Water Stress Index (CWSI) proposed by Jackson et al. (1981, 1988). In the SEBI concept, the dependence of the external resistance (to be defined below) on the atmospheric stability is considered. Additionally, SEBI is formulated as a pixelwise parameter. Subsequently it has been extended or refined to be applicable to satellite imagery in combination with Planetary Boundary Layer (PBL) parameters from numerical weather prediction models (Menenti et al., 2001; Van den Hurk and Su, 1999). In general terms SEBI is based on the calculation of a minimum and a maximum reference surface temperature under given radiative and atmospheric forcing. The general idea is that at given net radiation and within an area where the atmospheric conditions may be assumed constant, surface temperature is directly related to the ratio of actual to maximum land evaporation.

The general derivation is based on a combination equation for evaporation proposed by Menenti (1984) which, when the resistances terms are grouped into internal (or surface, or stomatal) and external resistances, can be shown to reduce to the widely used Penman-Monteith equation (Monteith, 1992) in the following form

$$\lambda E = \frac{\Delta \cdot r_e \cdot (R_n - G_0) + \rho C_p \cdot (e_{sat} - e)}{r_e \cdot (\gamma + \Delta) + \gamma \cdot r_i} \tag{2-12}$$

where e and e_{sat} are vapour pressure and saturated vapour pressure respectively; γ is the psychrometric constant, and Δ is the rate of change of saturation vapour pressure with temperature (i.e. $\partial e_s(T)/\partial T$); r_i is the bulk surface internal resistance and r_e is the

external or aerodynamic resistance. In the above equation it is assumed that the roughness length for heat and vapour transfer are the same (Brutsaert, 1982). It should be pointed out, that the Penman-Monteith equation is strictly only valid for vegetation canopy, whereas the definition by means of Eq. (2-12) is also valid for soil surface for properly defined internal resistance.

The actual external resistance depends on the actual Obukhov length L, which in turn is a function of the friction velocity and actual sensible heat flux. With the friction velocity and the Obukhov length determined by a numerical procedure described by Su at al. (2000), the actual value of the external resistance can be determined as

$$r_e = \frac{1}{ku_*}\left[\ln\left(\frac{z-d}{z_{0h}}\right) - \Psi_h\left(\frac{z-d}{L}\right) + \Psi_h\left(\frac{z_{0h}}{L}\right)\right] \tag{2-13}$$

The difficulty in using Eq. (2-12) to evaluate evaporation lies in the fact that the internal resistance, r_i, is generally regulated by the internal surface moisture availability which is in turn influenced by evaporation. However, for a completely wet surface it can be assumed that r_i = 0, indicating that the evaporation occurs at maximum controlled by the available radiation and the atmospheric forcing. While on the other hand, for a completely dry surface, it is assumed that r_i = ∞, meaning no evaporation.
Further it has been shown that the combination equation can be written to give explicitly the difference, $(T_0 - T_a)$, between the surface temperature and the reference temperature (Jackson *et al.*, 1981,1988; Stanghellini, 1987; Menenti and Choudhury, 1993).

$$(T_0 - T_a) = \frac{[(r_e + r_i)(R_n - G_0)/(\rho C_p)] - (e_{sat} - e)/\gamma}{1 + \Delta/\gamma + r_i/r_e} \tag{2-14}$$

In the present study, we will extend upon the work by Van den Hurk and Su (1999) to determine the relative evaporation by scaling an observed surface temperature in a maximum range of surface temperatures, defined by extremes in the surface energy balance. Several aspects differ from previous related work. The determination of actual resistance is based on the model for the determination of the roughness length for sensible heat transfer proposed by Su *et al.* (2000). The extreme cases of completely dry and completely wet are based on energy balance considerations, including the influences of the stability respectively. This has the advantage that the feedback effects between land surface and the overlaying atmospheric layer are considered. Using either surface layer scaling (MOS scaling) or the planetary boundary layer scaling (BAS scaling), it is possible to define the maximum and minimum temperature differences between the surface and reference layer, respectively.

In the following, we will define the relevant variables at the dry and wet limits respectively.

A) Dry limit
Under completely dry conditions, the sensible heat flux, H_d, can be derived from Eq. (2-1) as:

$$H_d = R_n - G_0 \tag{2-15}$$

This is equivalent to state that for a surface where no evaporation takes place because of lack of water, all available energy is used for heating the atmosphere.

Under such conditions, the dry-limit stability length can be obtained as

$$L_d = -\frac{\rho C_p u_*^3 \overline{\theta_v}}{kg(R_n - G_0)} \tag{2-16}$$

where $\overline{\theta_v}$ is the average of the potential temperature at the surface and at the reference height. The dry-limit external resistance and the dry-limit temperature difference between the surface and the overlaying air (for r_i = ∞) are given by

$$r_{ed} = \frac{1}{ku_*}\left[\ln\left(\frac{z-d}{z_{0h}}\right) - \Psi_h\left(\frac{z-d}{L_d}\right) + \Psi_h\left(\frac{z_{0h}}{L_d}\right)\right] \tag{2-17}$$

and

$$(T_0 - T_a)_d = r_{ed}\frac{R_n - G_0}{\rho C_p} \tag{2-18}$$

respectively.

B) Wet limit

On the other hand, when the surface is completely wet, the sensible heat flux reduces to its minimum value by means of:

$$H_w = R_n - G_0 - \lambda E_w \tag{2-19}$$

which from energy consideration may be approximated as $H_w \approx 0$.

Correspondingly at the wet limit where maximum evaporation occurs (i.e. r_i = 0), we get the wet-limit stability length

$$L_w = -\frac{\rho C_p u_*^3 \overline{\theta_v}}{kg \cdot 0.61 \cdot (R_n - G_0)/L_e} \tag{2-20}$$

where L_e is the latent heat of vaporization. The wet-limit external resistance is given as

$$r_{ew} = \frac{1}{ku_*}\left[\ln\left(\frac{z-d}{z_{0h}}\right) - \Psi_h\left(\frac{z-d}{L_w}\right) + \Psi_h\left(\frac{z_{0h}}{L_w}\right)\right] \tag{2-21}$$

and the wet-limit temperature difference is given as

$$(T_0 - T_a)_w = \left(r_{ew} \cdot \frac{R_n - G_0}{\rho C_p} - \frac{e_s - e}{\gamma}\right) \Big/ \left(1 + \frac{\Delta}{\gamma}\right) \tag{2-22}$$

Following Menenti and Choudhury (1993), the relative evaporation may now be expressed by evaluating the normalized actual temperature gradient with reference to the theoretical limits as

$$\Lambda_r = \frac{\lambda E}{\lambda E_w} = 1 - \frac{\dfrac{(T_0 - T_a)}{r_e} - \dfrac{(T_0 - T_a)_w}{r_{ew}}}{\dfrac{(T_0 - T_a)_d}{r_d} - \dfrac{(T_0 - T_a)_w}{r_{ew}}} \tag{2-23}$$

The maximum evaporation, λE_w, can be obtained from Eq. (2-12) by setting r_i = 0.

The evaporative fraction is finally given by:

$$\Lambda = \frac{\lambda E}{R_n - G} = \frac{\Lambda_r \cdot \lambda E_w}{R_n - G} \tag{2-24}$$

Using the previous energy consideration approximation, it becomes obvious that $\Lambda \approx \Lambda_r$.

The present scheme differs in three aspects from previous SEBI formulations. Firstly, a pixelwise calculation of radiation balance, maximum temperature range and actual evaporative fraction is applied, rather than the use of the same range for all pixels within a NWP model grid cell. Secondly, the model proposed by Su et al. (2000) is applied to derive pixelwise z_{0h} instead of using a fixed kB^{-1} value. This has been shown very important in deriving the sensible heat flux. Previously, the value of z_{0h} had to be obtained by assuming a constant kB^{-1} value and optimising the relationship between the aerodynamic roughness z_{0m} and a vegetation index (Van den Hurk and Su 1999; Pelgrum, 2000). Thirdly, newly proposed MOS or BAS stability corrections by Brutsaert (1999) are applied, rather than an empirical interpolation between two supposed extreme values of L_d and L_w, which can influence the evaporative fraction in important ways. The definition of z_{0h} is quite crucial in the application of SEBI. It affects both $(T_0 - T_a)_w$ and r_e, and thus the relative position of the observed $(T_0 - T_a)/r_e$ within the possible range.

2.5. The energy balance consideration for determination of evaporative fraction

Based on purely energy balance considerations, we can propose the following formulations.

Under the dry-limit, the sensible heat flux is at its maximum value, i.e.

$$H_{\max} = R_n - G_0 \tag{2-25}$$

Under the wet-limit, it will take its minimum value

$$H_{\min} = \left((R_n - G_0) - \frac{\rho C_p}{r_{ew}} \cdot \frac{e_s - e}{\gamma} \right) \Big/ \left(1 + \frac{\Delta}{\gamma} \right) \tag{2-26}$$

The relative evaporation then can be evaluated as

$$\Lambda_r = 1 - \frac{H - H_{\min}}{H_{\max} - H_{\min}} = 1 - \frac{\rho C_p \frac{(T_0 - T_a)}{r_e} - H_{\min}}{H_{\max} - H_{\min}} \tag{2-27}$$

The evaporative fraction is again defined by Eq. (2-24). It is trivial to observe that the results from this formulation and that based on the SEBI formulation are identical.

2.3 Conclusions

In this contribution we have described the Surface Energy Balance System (SEBS) for the estimation of atmospheric turbulent fluxes and surface evaporation using satellite earth observation data in the visible, near infra-red, and thermal infrared frequency range.

Based on a limited set of case studies using point measurements, SEBS has proven to be capable to estimate turbulent heat fluxes from point to continental scale with acceptable accuracy (Su, 2001). The applications of SEBS to high resolution remote sensing data will be dealt with in the next three chapters.

3 Estimation of evaporation using SEBS - EFEDA

(Z. Su, C. Jacobs)

Abstract
The Surface Energy Balance System (SEBS) (Su, 2000; Chapter 2) is applied in this contribution to a Thematic Mapper Simulator (TMS) scene collected in Barrax, during the EFEDA campaign. Firstly a brief review is given to a set of necessary inputs for SEBS. These inputs include among others, surface albedo, vegetation indices, emissivity, temperature, roughness and incoming global radiation. Then these inputs are used to derive the evaporative fraction using SEBS. A preliminary comparison is performed between the derived evaporative fraction and limited in-situ point measurement data. SEBS is shown to perform satisfactorily.

3.1 Introduction

In this contribution we will apply the SEBS to a Thematic Mapper Simulator (TMS) scene collected in Barrax, during the EFEDA campaign. Firstly a brief review is given to a set of necessary inputs for SEBS. These inputs include among others, surface albedo, vegetation indices, emissivity, temperature, roughness and incoming global radiation. Then these inputs are used to derive the evaporative fraction using SEBS. A preliminary comparison is performed between the derived evaporative fraction and limited in-situ point measurement data.

Table 3-1. Characteristics of the TMS-NS001 data which contain the seven Landsat TM bands plus a band from 1.13 to 1.35 μm (band 5). Only the bands corresponding to Landsat TM bands are used in this study. The TMS-NS001 was on board of NASA's ER2, 29 June 1991, 12.21 GMT, Barrax, Spain, with 18.5m ground resolution ($K(\lambda)$ is the normal incoming spectral solar irradiance and $L_{\min}(\lambda)$ and $L_{\max}(\lambda)$ are minimum and maximum spectral radiance, respectively).

Band	Wavelength range λ (μm)	Bandwidth $\Delta\lambda$ (μm)	$K(\lambda)$ (mw.cm^{-2}. μm^{-1})	$L_{\min}(\lambda)$ (mw.cm^{-2}.sr^{-1} . μm^{-1})	$L_{\max}(\lambda)$ (mw.cm^{-2}.sr^{-1} . μm^{-1})
1	0.458-0.519	0.07	136.93	-0.15	15.21
2	0.529-0.603	0.08	148.20	-0.28	29.68
3	0.633-0.697	0.06	92.64	-0.12	20.43
4	0.767-0.910	0.14	148.64	-0.15	20.62
6	1.57-1.71	0.20	46.17	-0.037	2.719
7	2.10-2.38	0.27	14.97	-0.015	1.438
8	10.9 -12.3	5.50	0.0325	0.1238	1.5600

3.2 Data and study area

Data obtained with the Thematic Mapper Simulator (TMS-NS001) during the EFEDA campaign (Bolle *et al.,* 1993) for the Barrax region, Spain of 29 June 1991 is used. In addition, radiosonde and surface tower flux, as well as surface radiation measurements are used, where appropriate, to determine regionally constant parameters. These parameters include atmospheric transmissivity, potential air temperature at the blending height and the incoming long wave radiation at the time of the remote sensing data collection. The characteristics for TMS-NS001 are shown in table 3-1.

The TMS image of 29 June 1991 is shown in figure 3-1. The spatial resolution of the data is 18.5 m. The circular shapes in the scene are due to pivot irrigation. Fields and roads can be seen clearly. The two lines running top to bottom in the middle of the image indicate missing data.

Figure 3-1. Barrax, 29 June 1991, TMS-NS001 (bands: 4,5,3)

3.3 The surface energy balance system applied to TMS data

The details of the Surface Energy Balance System (SEBS) have been given by Su (Chapter 2). We will only describe the specifications used in generating evaporative fractions using the TMS data and radiosonde data.

Primary inputs to SEBS

A. Remote sensing physical parameters derived from TMS data
A1. albedo (-)
A2. Potential surface temperature (K)
A3. Normalized Difference Vegetation Index (-)
A4. emissivity (-)
A5. LAI, vegetation fractional coverage and roughness length for momentum transfer

B. Radiosonde and Surface in-situ data
B1. clear sky downward shortwave radiation ($W.m^{-2}$)
B2. clear sky downward longwave radiation ($W.m^{-2}$)
B3. PBL-height (m)
B4. Surface pressure (Pa)
B5. PBL-averaged specific humidity ($kg.m^{-3}$)
B6. PBL-averaged potential temperature (K)
B7. PBL-averaged horizontal wind speed ($m.s^{-1}$)

The relevant parameters for this study are given in Table 3-2.

Table 3-2. Input parameters for application of SEBS to the TMS data.

Surface temperature (^0C)	TMS derivative
Surface albedo (-)	TMS derivative
NDVI (-)	TMS derivative
PBL Depth (m)	750
PBL pressure (Pa)	85986.1
PBL potential temperature (K)	300.15
PBL specific humidity ($kg.kg^{-1}$)	0.0093,
PBL wind speed ($m.s^{-1}$)	8.0
Surface pressure (Pa)	94000.0
Downward long-wave radiation ($W.m^{-2}$)	372.0
Surface short-wave clear sky radiation ($W.m^{-2}$)	860.0

3.4 Results and discussions

3.4.1 Input parameters

We will now describe the methods to derive the input parameters to SEBS from remotely observables.

Incoming global radiation

Incoming global radiation is calculated according to

$$K^{\downarrow} = e_0 I_{sc} \cos(\theta) \cdot \tau_a \qquad (3\text{-}1)$$

where I_{sc} = 1367 ($W.m^{-2}$) (Iqbal, 1983) is the solar constant and τ_a is the total atmospheric transmissivity which can be derived using measured surface incoming global radiation and is assumed spatially constant over the whole region. Since the study area is small and flat, there will be no big spatial difference in the incoming global radiation field.

Surface albedo

Using field measured surface albedo, α, Bastiaanssen (1995) found:

$$\alpha = -0.085 + 1.47 r_p \qquad (3\text{-}2)$$

where r_p is the reflectance value at the appropriate height, which, for simplicity, may be called the planetary reflectance. r_p is calculated as follows:

$$r_p(\lambda) = \frac{\pi L(\lambda)}{e_0 K(\lambda)\cos(\theta)} \tag{3-3}$$

where $L(\lambda)$ is the measured spectral radiance at wavelength λ, e_0 is the eccentricity factor that takes into account the average and actual earth-sun distances, $K(\lambda)$ is the normal incoming spectral solar irradiance and θ is the solar zenith angle.

$$L(\lambda) = L_{\min}(\lambda) + (L_{\max}(\lambda) - L_{\min}(\lambda))\frac{DN(\lambda)}{255}. \tag{3-4}$$

$L_{\min}(\lambda)$ and $L_{\max}(\lambda)$ are the minimum and maximum spectral radiance, DN(λ) is the recorded digital number. The constants are given in Table 3-1.

The integrated broad band planetary reflectance is calculated using (Menenti et al., 1989)

$$r_p = \sum w(\lambda) r_p(\lambda) \tag{3-5}$$

The weighting factors, $w(\lambda)$, can be calculated using bands 1-4,6-7 and the information provided in EOSAT Technical Note (1986) and Iqbal (1983).

Vegetation index

The normalized difference vegetation index (NDVI) is used, which can be calculated as

$$NDVI = \frac{L(\lambda_4) - L(\lambda_3)}{L(\lambda_4) + L(\lambda_3)}. \tag{3-6}$$

Surface emissivity

The relationship proposed by Van de Griend and Owe (1993) is used; this reads

$$\varepsilon = 1.009 + 0.047 \ln(NDVI) \tag{3-7}$$

which is valid for NDVI=0.16-0.74. This equation is empirical and is valid only for the conditions under which the measurements have been made. The conditions in this study are similar to those under which the equation was derived.

Surface temperature

Given the measured thermal infrared radiance, L_t, or the converted radiometric temperature, T_r, the surface temperature, T_0, can be derived from the following equations

$$\varepsilon \sigma T_0^4 = \sigma T_r^4 \tag{3-8}$$

The radiometric temperature can be derived according to EOSAT Tech. Note (1983)

$$T_r = \frac{K_2}{\ln(K_1/L_t + 1)} \tag{3-9}$$

where K_2=1260.56 mW.cm^{-2}.sr^{-1}.µm^{-1} and K_1=60.776 mW.cm^{-2}.sr^{-1}.µm^{-1} are calibration constants.

LAI, vegetation fractional coverage and roughness length for momentum transfer

Here we use a simple formula synthesized from Su (1996, 2000) to derive the leaf area index (LAI), since more accurate formulas are not available for the time being:

$$LAI = \left(NDVI \cdot \frac{1 + NDVI}{1 - NDVI + \delta NDVI} \right)^{1/2} \tag{3-10}$$

This formula is strictly only good for low vegetation since NDVI saturates at higher LAI values. However, there is not sufficient information for the study area to support more sophisticated formulations.

The fractional vegetation coverage is calculated as follows:

$$f_c = \left(\frac{NDVI - NDVI_{\min}}{NDVI_{\max} - NDVI_{\min}} \right) \tag{3-11}$$

where $NDVI_{\min}$ is the NDVI for bare soil and $NDVI_{\max}$ for full vegetation coverage.
A simple relationship is used to derive the roughness length for momentum transfer as follows

$$z_{0m} = 0.005 + 0.5 \cdot \left(\frac{NDVI}{NDVI_{\max}} \right)^{2.5} \tag{3-12}$$

Using field measured z_0, a relationship was found as (Bastiaanssen, 1995)

$$z_{0m} = \exp(-5.2 + 5.3 \cdot NDVI) \tag{3-13}$$

The values derived from the above two expressions are practically the same when $NDVI \leq 0.7$. However, when $NDVI \approx 1.0$, the latter gives $z_{0m} > 1.0\ m$, which is much too big for low vegetation when compared to literature recommendations (e.g. Wieringa, 1993). The maximum value given by the former is 0.5 for $NDVI \approx 1.0$, which we consider more realistic for the present situation and thus will be used in this study.

A conversion is performed according to Brutsaert (1982) to derive vegetation height and displacement height for a given aerodynamic roughness height.

$$h = \frac{z_{0m}}{0.136} \tag{3-14}$$

$$d = \frac{2}{3} h \tag{3-15}$$

Some constants for vegetation are given as follows: C_d = 0.2, the canopy drag coefficient; C_t = 0.01, the leaf heat transfer coefficient; D_l = 0.05 (m), the leaf width.

Evaporative fractions

Having prepared the required inputs and parameters, the following steps are followed to derive the pixelwise evaporative fractions.

The model of Su *et al.* (2000) is used to derive the roughness height for heat transfer;

The Bulk Atmospheric Similarity (BAS) is used to derive the friction velocity, the sensible heat flux and the Obukhov length.

Finally, the SEBI option within SEBS is used to calculate the pixelwise evaporative fractions.

3.4.2 Results of the TMS data

The result of the SEBS calculations is shown in figure 3-2. The corresponding histogram of the calculated evaporative fractions is shown in figure 3-3.

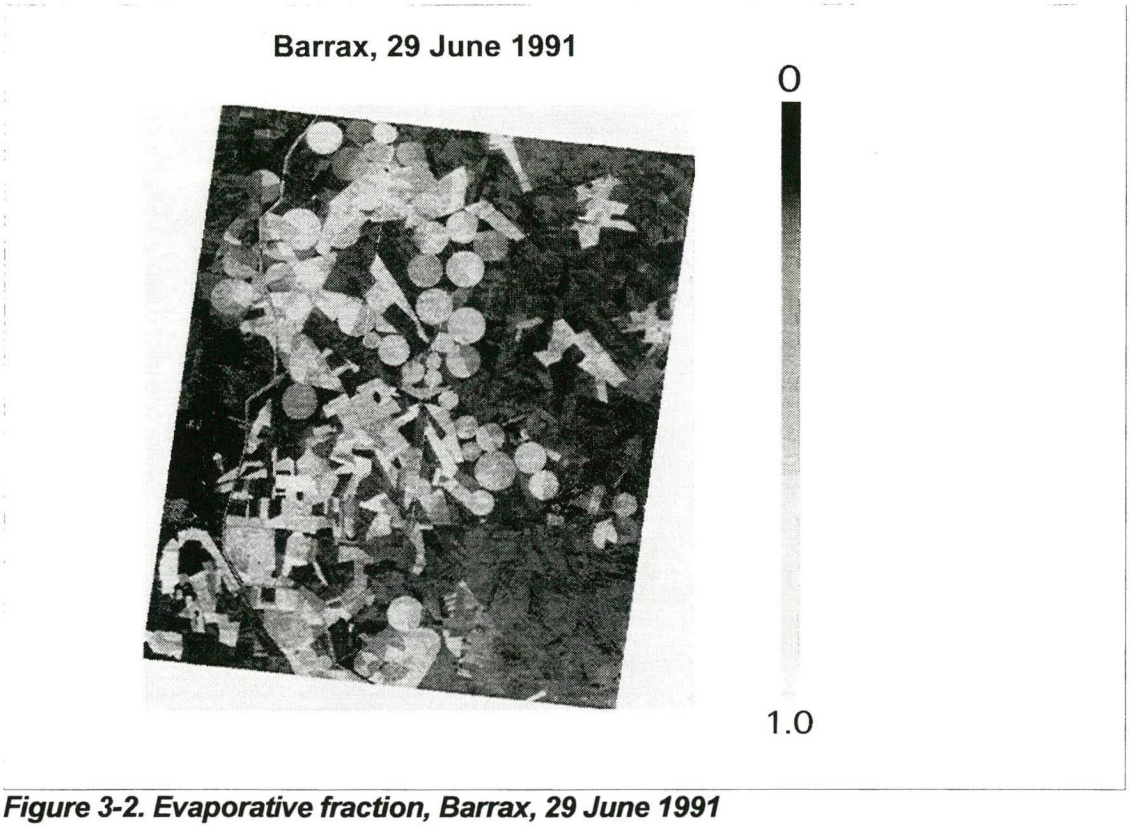

Figure 3-2. Evaporative fraction, Barrax, 29 June 1991

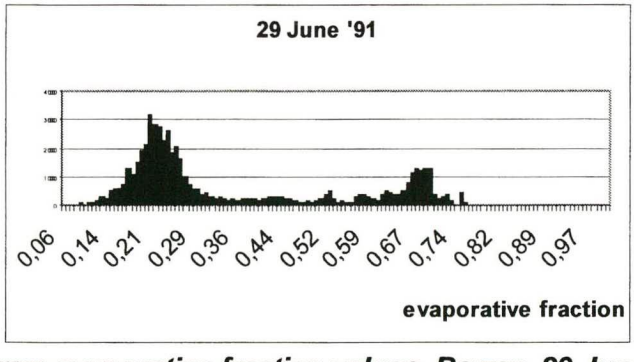

Figure 3-3. Histogram evaporative fraction values, Barrax, 29 June 1991.

3.4.3 Comparison SEBS results to field measurements

At three different surfaces in Barrax simultaneous field measurements of heat flux densities have been obtained (HAPEX EFEDA campaign): (1) irrigated maize, (2) fallow and (3) bare soil. Measurements at the maize and the fallow site have been performed by the University of Karlsruhe, and measurements at the bare soil site have been done by CNRM.

Figure 3-4 shows the comparison between the values for Λ obtained from field measurements and from SEBS for the three different surface types. The actual values are given in Table 3-3, together with the standard deviation of the SEBS estimates.

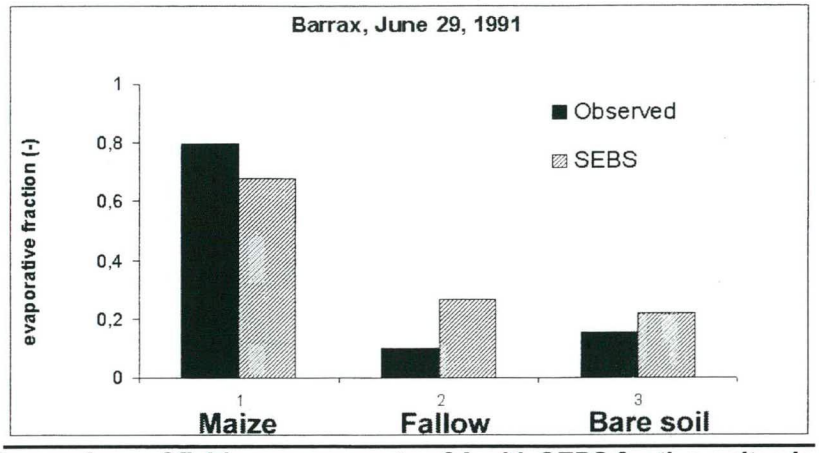

Figure 3-4: Comparison of field measurements of Λ with SEBS for three sites in the Barrax area, June 29, 1991.

Table 3-3: Comparison SEBS estimates of Λ with field measurements in the Barrax area, June 29, 1991

		x	y	measured	calculated	Sta.dev. calculated
Maize	Karlsruhe	372	483	0,798	0,682	0,003
Fallow	Karlsruhe	473	420	0,0984	0,266	0,125
Bare	CNRM	367	462	0,154	0,218	0,027

3.5 Discussions and conclusions

In this study, we have developed a set of methods for deriving land surface parameters. The SEBS is applied to a TMS scene in combination with PBL information from radiosonde data.

The SEBS estimates of the evaporative fractions are confined between 0 and 1. In the Barrax area, there is a clear distinction between irrigated crops and non irrigated/fallow/bare parts. Two clear peaks appear in the histogram: one peak around Λ = 0.25 (fallow) and a smaller one around Λ = 0.70 (irrigated crops). Furthermore, looking at the pivot circles and the corresponding Λ values, the efficiency of the irrigation can be inferred.

The comparison of the SEBS estimates to field measurements is satisfactory. The relatively small differences can be explained by the differences in measurement heights, the fetch areas and method of measurement. Further, since the SEBS estimates are instantaneous values based on the remote sensing data, while the in-situ measurements are half-hourly averages, difference should also occur due to the turbulent nature of the heat fluxes.

In the present study we have not been able to investigate the details of the quality of the input due to time constraints. Although various studies have used the TMS for various purposes (Bastiaanssen, 1995; Su *et al.*, 2000, Pelgrum, 2000) and the TMS data should be of good quality in terms of calibration and various corrections, some of the secondary

inputs have to be derived using rather limited knowledge of the surface conditions and of actual physical relationships. It is expected that such analysis will reveal valuable information as regards to the necessary accuracy in the derived input data.

Finally, it should be pointed out that the application of SEBS does not require any a priori knowledge of the actual turbulent heat fluxes. We have just derived the necessary input data from the TMS data and the radiosonde data and applied them to SEBS. This indicates SEBS is a credible and independent approach.

4 Estimation of evaporation using SEBS - Tuscany

(G.J. Roerink, M. Menenti, Z. Su)

Abstract
A small field campaign was conducted during August 1997 in the Piano di Rosia area in Tuscany, Italy. The terms of both the radiation balance and the surface energy balance were measured by several techniques and for several field sites. Together with a Landsat TM scene of 23 August 1997 of the same area, these data give an excellent opportunity for a profound study of interaction between the radiation and energy fluxes from point to regional scale. SEBS is applied to this TM scene to derive the surface energy fluxes. The results of SEBS are tested and validated with the available data.

4.1 Introduction

The exchange processes between land and atmosphere are of crucial importance for the re-distribution of moisture and heat in soil and atmosphere. The land surface connects the radiation, energy and water balances of the soil and atmosphere. To improve the understanding of these exchange processes the utilisation of satellite remote sensing is indispensable to extrapolate in-situ measurements to a regional scale. Landsat TM data can be compared directly with field measurements, because of its high resolution.

A small field campaign within the framework of the RESMEDES (Remote Sensing of Mediterranean Desertification and Environmental Stability) project was conducted during August 1997 in the Piano di Rosia area in Tuscany, Italy. The terms of both the radiation balance and the surface energy balance were measured by several techniques and for several field sites. Together with the Landsat TM scene of 23 August 1997 of the same area this gives an excellent opportunity for a profound study of interaction between the radiation and energy fluxes.

The SEBS (Su, this issue) is applied to derive the surface energy fluxes from remote sensing measurements. The results are tested and validated with the available data.

4.2 Material and method

The materials used in this study are the same as those used by Roerink *et al.* (2000). We will give a brief description of the necessary data sets, of which the full details can be found in Roerink *et al.* (2000).

4.2.1 Landsat TM data

During the small RESMEDES field campaign in the Piano di Rosia area in Tuscany, Italy the Landsat TM sensor passed by on 23 August 1997, 9:30:54 GMT. A colour composite of bands 4, 5 and 3 is shown in Fig. 4-1, together with a subset of the Piano di Rosia area, where the field campaign took place.

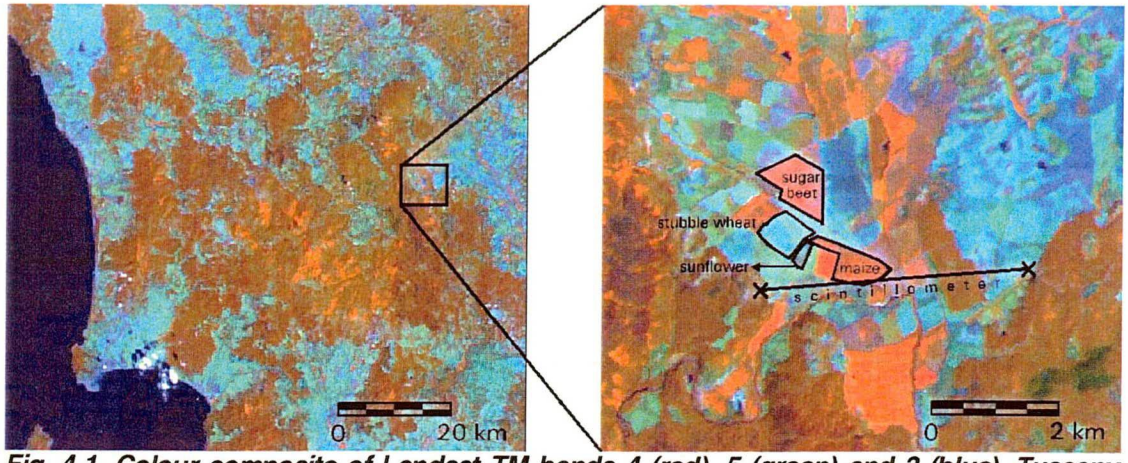

Fig. 4-1. Colour composite of Landsat TM bands 4 (red), 5 (green) and 3 (blue), Tuscany, Italy, 23 August 1997. The enlarged subset encompasses the Piano di Rosia area, where the field campaign took place.

4.2.2 DEM data

Tuscany is a hilly area, therefore a Digital Elevation Model (DEM) is necessary to correct for the solar incidence angle at the surface and the cooling effect of altitude on temperature. Two types of DEM's are available, the first one covers the whole Landsat TM area with a resolution of 250 m, the second type are DEM's of several Tuscany sub-areas of approximately 10x10 km with a resolution of 20 m.

To make use of all available DEM sources first slope and aspect are calculated for every DEM, whereafter they are resampled to the Landsat TM scale. Finally the 10x10 km sub-areas (of 20 m resolution) are mosaiced with the whole area covering DEM (of 250 m resolution).

4.2.3 Field campaign

Ground truth data were collected during a small field campaign in the Rosia di Piano area in Tuscany, August 1997. The terms of the radiation and the surface energy balance were measured at 4 sites: sugar beet, maize, sunflower and wheat stubble. Fig. 4-1 shows the Landsat TM image overlaid with the boundaries of the field sites. On a larger scale the sensible heat flux was measured with a scintillometer; this is a device measuring the refraction index of air, which can be related to temperature fluctuation and subsequently the sensible heat. For a detailed description, see De Bruin *et al.* (1995).

The measured data around the overpass time of Landsat TM are presented in table 4-1, with as well an assumed value for surface albedo and emitted longwave radiation (=black body surface radiation temperature) of open water (Mediterranean sea), in order to enlarge the range for calibrating the planetary measurements.

A few remarks are made here about the quality of the field data. First of all it can be seen that the terms of the radiation balance are stable in time as the mean 9:00-10:00 values correspond within a few W/m^2 units with the 9:30-9:31 values. The radiation balance terms used for calibration and validation of the Landsat TM flux calculations are hourly averaged values, since the one-minute values are only available for the sugar beet site. The energy balance terms are less stable, some increase with time while others decrease. However an increase related to the net radiation is expected. If the net radiation derived from the radiation balance is compared to the net radiation derived from the

energy balance, large discrepancies can be detected. For the maize site the difference is up to 160 W/m^2. Several reasons exist for these large discrepancies:

- In the field, different measurement techniques are used, which are based on different principles and have different accuracies.
- The sizes of the measured areas differ a lot within a single field site; radiation is hemispherically measured, the soil heat flux over an area of several cm^2 to a few dm^2 and the sensible and latent heat flux have a footprint in the upwind direction from several metres to a few kilometres.
- The chaotic nature of the turbulent fluxes (sensible and latent heat flux).

This should be taken into consideration when using the field measurements. Since the 9:00-9:30 GMT values of energy fluxes have the smallest discrepancies with the hourly averaged net radiation, these values are taken for validation of the fluxes.

Table 4-1. Measured field data on 23 August 1997, where Bowen = Bowen ratio measurement; eddy = eddy correlation measurement; LAS = Laser Aperture Scintillometer measurement and residual = rest term of radiation or energy balance.

Land surface parameter	Sugar beet	Maize	Sunflower	Wheat stubble	Valley	Sea water
Incoming sw radiation						
9:00-9:30 GMT	726.33	same as	Same as			
9:30-10:00 GMT	774.50	sugarbeet	Sugarbeet			
9:30-9:31 GMT	755.30					Surface albedo estimated at 0.05 (-)
Reflected sw radiation						
9:00-9:30 GMT	129.01	116.19	107.59			
9:30-10:00 GMT	135.08	120.82	115.90			
9:30-9:31 GMT	132.66					
Incoming lw radiation						
9:00-9:30 GMT	347.88	same as	same as			
9:30-10:00 GMT	353.63	sugarbeet	sugarbeet			
9:30-9:31 GMT	352.96					Surface temp. estimated at 20 °C from SST
Emitted lw radiation		(residual)	(residual)			
9:00-9:30 GMT	464.43	462.21	482.47			
9:30-10:00 GMT	471.07	472.32	498.50			
9:30-9:31 GMT	468.45					
Net radiation	(residual)					
9:00-9:30 GMT	480.76	495.81	484.15			
9:30-10:00 GMT	521.98	534.99	513.73			
9:30-9:31 GMT	507.15					
Soil heat flux						
9:00-9:30 GMT	37.41	18.39	51.73			
9:30-10:00 GMT	43.06	20.40	57.58			
Sensible heat flux	(Bowen)	(eddy)	(eddy)	(eddy)	(LAS)	
9:00-9:30 GMT	100.28	63.02	181.51	205.05	135.17	
9:30-10:00 GMT	111.76	58.42	137.24	172.91	160.70	
9:25-9:30 GMT					160.44	
Latent heat flux	(Bowen)	(eddy)	(residual)			
9:00-9:30 GMT	309.48	331.33	250.91			
9:30-10:00 GMT	327.61	291.66	318.91			
Wind speed						
9:00-9:30 GMT		0.77	0.41	0.91		
9:30-10:00 GMT		0.65	0.49	0.55		
9:30-9:31 GMT		0.41				

4.2.4 The Surface Energy Balance System applied to TM data

The details of the Surface Energy Balance System (SEBS) have been given in Chapter 2. We will only describe the specifications used in generating evaporative fractions using the TM data and in-situ data.

Primary inputs to SEBS are:

A. Remote sensing physical parameters derived from TM data
A1. albedo (-)
A2. Potential surface temperature (K)
A3. Normalized Difference Vegetation Index (-)
A4. Emissivity (-)
A5. LAI, vegetation fractional coverage and roughness length for momentum transfer

B. Radiation and in-situ data
B1. Reference height (m) (height of scintillometer above sea level)
B2. Potential temperature at reference height (K)
B3. Actual surface vapour pressure (Pa)
B4. Wind speed at reference height (m/s)
B5. Height of surface above sea level (m)
B6. Downward long-wave radiation (W/m^2)
B7. Surface short-wave clear sky radiation (W/m^2)

The reference height is taken as the height of the scintillometer. Other parameters are derived from in-situ data.The wind speed from the measurement mast is extrapolated to the reference height assuming neutral stability. The relevant parameters for this study are given in Table 4-2.

Table 4-2. Input parameters for application of SEBS to the TMS data.

Surface temperature (^0C)	TM derivative
Surface albedo (-)	TM derivative
NDVI (-)	TM derivative
Emissivity (-)	TM derivative
Reference height (m) (height of scintillometer above sea level)	237.0
Potential temperature at reference height (K)	299.55
Actual surface vapour pressure (Pa)	0.0093
Wind speed at reference height (m/s)	2.86
Height of surface above sea level (m)	180.0
Downward long-wave radiation (W/m^2)	350.75
Surface short-wave clear sky radiation (W/m^2)	774.50

4.3 Results

4.3.1 Remote sensing physical parameters derived from TM data

Surface albedo

The surface albedo is determined from the 6 TM bands which measure the spectral reflectance in the visible and near and middle infra-red part of the electro-magnetic spectrum. First the broadband planetary albedo is calculated by means of a spectral weighing procedure and adjusted for the incidence angle. Afterwards the planetary albedo

is plotted against measured surface albedo and the transmittance and path radiance of the atmosphere is calculated. With aid of this transmittance, finally all pixels are given a surface albedo value depending linearly on their planetary albedo.

For each band first the spectral radiance is calculated using constant values:

$$L(\lambda) = a + \frac{(b-a)}{255} DN \qquad (4\text{-}1)$$

where:
L(λ) = spectral radiance for wavelength λ [mW cm^{-2} sr^{-1} μm^{-1}]
DN = Digital Number [-]

The constants a and b are given by Markham & Barker (1987) and are presented in Table 4-3.

Table 4-3. Landsat TM band specific constants

Band	a	b	$K^{\downarrow}(b)$	Weight
1	-0.15	15.21	195.7	0.293
2	-0.28	29.68	182.9	0.274
3	-0.12	20.43	155.7	0.233
4	-0.15	20.62	104.7	0.156
5	-0.037	2.719	21.93	0.033
7	-0.015	1.438	7.452	0.011

The corresponding planetary albedo for each band:

$$r_p(b) = \frac{\pi L(\lambda) d^2}{K^{\downarrow}(b) \cos\varphi_s} \qquad (4\text{-}2)$$

where:
d = relative earth-sun distance [-]
$K^{\downarrow}(b)$ = incoming shortwave radiation at the top of the atmosphere for band b [mW cm^{-2} sr^{-1} μm^{-1}]
φ_s = solar zenith angle [rad]

The slope and aspect maps derived from the DEM provide the necessary information to calculate the solar zenith angle, e.g. the angle between the incoming solar ray and the normal to the (hilly) surface. For flat surfaces the solar zenith angle is 38.7° in this TM-scene. The incoming shortwave radiation at the top of atmosphere differs per band, according to Table 4-3. The broadband planetary albedo is being calculated as the total sum of the different in-band planetary reflectance according to different weights for different bands, which can be found also in Table 4-3.

Now the relation between surface albedo and planetary albedo can be established by plotting measured surface albedos (ratio of measured reflected shortwave radiation over measured incoming shortwave radiation, see Table 4-3) against corresponding calculated planetary albedos and perform a linear regression through the points. The fitted relationship is: $r_0 = 1.864 * r_p - 0.030$.

<u>Surface temperature</u>

Band 6 (10.4 - 12.5 μm) of Landsat TM measures emitted long-wave radiation from the earth surface and atmosphere. DN-values of band 6 are converted to spectral radiance at top of atmosphere ($L_{6,TOA}(\lambda)$) by:

$$L_{6,TOA}(\lambda) = 0.1238 + \frac{1.560 - 0.1238}{255} DN \tag{4-3}$$

Satellite temperature (T_{sat}) is derived from the spectral radiance by:

$$T_{sat} = \frac{1260.56}{\ln(\frac{60.776}{L_{6,TOA}(\lambda)} + 1)} \tag{4-4}$$

The different constants in Eqs. (4-3) and (4-4) can be found in Markham and Barker (1987). Applying the Stefan-Boltzmann law, the outgoing long-wave radiation at the top of atmosphere $L^{\uparrow}_{TOA}$ is:

$$L^{\uparrow}_{TOA} = \sigma T^4_{sat} \tag{4-5}$$

Where σ is the Stefan-Bolzmann constant ($5.67*10^{-8}$ W m^{-2} K^{-4}). Now the outgoing longwave radiation at the top of atmosphere (TOA) can be atmospherically corrected by linking the outgoing longwave radiation at the top of atmosphere to the outgoing longwave radiation at the surface, $L^{\uparrow}$. The value for open water is added in order to enlarge the calibration range, it is taken from http://podaac.jpl.nasa.gov/sst/, as the mean Sea Surface Temperature of August, 1997. The measured Maize value is not used in the fit, because it is measured as the rest term of the radiation balance, and therefore an accumulation of all measured errors. The linear regression gave:

$$L^{\uparrow} = 0.607 L^{\uparrow}_{TOA} + 170.405 \tag{4-6}$$

The radiative surface temperature, T_0^R, is calculated by inverting the Stefan-Boltzmann law:

$$T_0^R = \sqrt[4]{(L^{\uparrow} / \sigma)} \tag{4-7}$$

The next step is to correct the radiative surface temperature for emissivity effects of the surface:

$$T_0 = \sqrt[4]{(T_0^{R4} / \varepsilon_0)} \tag{4-8}$$

Where ε_0 is the surface emissivity.

Normalised Difference Vegetation Index

The Normalised Difference Vegetation Index, NDVI, is calculated as:

$$NDVI = \frac{r_{p4} - r_{p3}}{r_{p4} + r_{p3}} \tag{4-9}$$

Where r_{p3} and r_{p4} are the planetary reflectances in band 3 and 4 respectively. No atmospheric correction is applied to the NDVI, since it is only used as one of the inputs for the empirical relationships of surface emissivity and soil heat flux, which have to be established anyway.

Emissivity

The vegetation cover method of Valor and Caselles (1996) is used to estimate the emissivity:

$$\varepsilon_0 = \varepsilon_v P_v + \varepsilon_g (1 - P_v) + 4\langle d\varepsilon \rangle P_v (1 - P_v) \tag{4-10}$$

with:

$$P_v = \frac{NDVI - NDVI_g}{NDVI_v - NDVI_g} \tag{4-11}$$

where:

ε_v = emissivity of full vegetation cover [-]
ε_g = emissivity of bare soil [-]
P_v = fractional vegetation cover [-]
$\langle d\varepsilon \rangle$ = vegetation structure parameter [-]
$NDVI_v$ = NDVI of full vegetation cover [-]
$NDVI_g$ = NDVI of bare soil [-]

With no additional information available the ε_g, ε_v and $\langle d\varepsilon \rangle$ terms in the spectral 8-14 μm region (band 6) are set at respectively 0.91, 0.99 and 0.02, according to Valor and Caselles (1996). From the NDVI histogram $NDVI_g$ and $NDVI_v$ were set at 0.1 and 0.8.

LAI, vegetation fractional coverage and roughness length for momentum transfer

Here we use a simple formula synthesized from Su (1996, 2000) to derive the leaf area index (LAI), since more accurate formulas are not available for the time being:

$$LAI = \left(NDVI \cdot \frac{1 + NDVI}{1 - NDVI + \delta NDVI} \right)^{1/2} \tag{4-12}$$

This formula is strictly only good for low vegetation since NDVI saturates at higher LAI values. However, there is not sufficient information over continental scale to support more sophisticated formulations. The fractional vegetation coverage is calculated as follows:

$$f_c = \left(\frac{NDVI - NDVI_{\min}}{NDVI_{\max} - NDVI_{\min}} \right) \tag{4-13}$$

where $NDVI_{\min}$ is the NDVI for bare soil and $NDVI_{\max}$ for full vegetation coverage.

A simple relationship is used to derive the roughness length for momentum transfer as follows

$$z_{0m} = 0.005 + 0.5 \cdot \left(\frac{NDVI}{NDVI_{\max}} \right)^{2.5} \quad (4\text{-}14)$$

Using field measured z_0, a relationship was found as (Bastiaanssen, 1995)

$$z_{0m} = \exp(-5.2 + 5.3 \cdot NDVI) \quad (4\text{-}15)$$

The values derived from the above two expressions are practically the same when $NDVI \leq 0.7$. However, when $NDVI \approx 1.0$, the latter gives $z_{0m} > 1.0\,m$, which is much too big for low vegetation when compared to literature recommendations (e.g. Wieringa, 1993). The maximum value given by the former is 0.5 for $NDVI \approx 1.0$, which we consider more realistic for the present situation and thus will be used in this study.

A conversion is performed according to Brutsaert (1982) to derive vegetation height and displacement height for a given aerodynamic roughness height.

Some constants for vegetation are given as follows: C_d = 0.2, the canopy drag coefficient; C_t = 0.01, the leaf heat transfer coefficient; D_l = 0.05 (m), the leaf width.

Evaporative fraction

Having prepared the required inputs and parameters, the following steps are followed to derive the pixelwise evaporative fractions.

The model of Su *et al.* (2000) is used to derive the roughness height for heat transfer; The Bulk Atmospheric Similarity (BAS) is used to derive the friction velocity, the sensible heat flux and the Obukhov length.

Finally, the SEBI option within SEBS is used to calculate the pixelwise evaporative fractions which are shown in Fig. 4-2.

The SEBS estimates of evaporative fraction for the sea water are slightly bigger than 1.0 which indicates an extra supply of energy to the sea water through advection of warmer air from the land. Over bare soils the evaporative fractions are generally around 0.0 or slightly negative, thus indicating a reverse process as at the sea. Vegetated surfaces have values of usually in the range of 0.5 ~ 0.9 which are qualitatively realistic.

4.3.2 Surface energy balance parameters

In producing the energy balance terms, the same procedure used by Roerink *et al.* (2000) is used instead of the actual SEBS parameterisations. Only the SEBS estimate of the evaporative fraction, Λ, is used. This is done for the ease to compare the present results to those of Roerink *et al.* (2000).

Net radiation

The energy source for the land surface flux densities G_o, H and λE is the net radiation flux density R_n, defined as the resultant of all incoming and outgoing radiation. The radiation balance can be expressed as:

$$R_n = K^{\downarrow} - K^{\uparrow} + L^{\downarrow} - L^{\uparrow} \quad (4\text{-}16)$$

Where the incoming sw radiation, $K^{\downarrow}$, is calculated according to its geographic coordinates, daynumber and daytime. The reflected sw radiation, $K^{\uparrow}$, is defined by the surface albedo, and the emitted lw radiation, $L^{\uparrow}$, is defined by the surface temperature according to Stefan-Boltzmann law. The only unknown term, the incoming lw radiation, $L^{\downarrow}$, is measured in the field and is 350.75 W m^{-2} (mean value from 9:00-10:00 GMT, see Table 4-3). Fig. 4-3(a) is the resulting map of the net radiation.

Soil heat flux

The soil heat flux, G_0, is the energy used for warming or cooling the subsurface soil volume. It is determined by the thermal conductivity of the soil and the temperature gradient of the topsoil. This cannot be directly determined through remote sensing techniques. Many investigations have shown that mid-day soil heat flux / net radiation fraction is reasonably predictable from remote sensing determinants of vegetation characteristics (Daughtry *et al.*, 1990). However, the attenuation of radiative and conductive heat transfer in canopy and soil respectively changes significantly with soil type. The expression used to define the soil heat flux density is:

$$G_0 = \Gamma R_n \tag{4-17}$$

with:

$$\Gamma = \frac{T_0 - 273.15}{r_0}\left(0.32r_0 + 0.62r_0^2\right)\left(1 - 0.978NDVI^2\right) \tag{4-18}$$

Where Γ (-) is the soil heat / net radiation flux density ratio, which is an empirical relationship of the surface reflectance, surface temperature and NDVI. Fig. 4-3(b) is the resulting map of the soil heat flux.

Sensible heat flux

The sensible heat flux is the heat transfer between the ground and the atmosphere. It is calculated from the net available energy and the evaporative fraction as:

$$H = (1 - \Lambda)(R_n - G_0) \tag{4-19}$$

Fig. 4-3(c) is the map of the sensible heat flux.

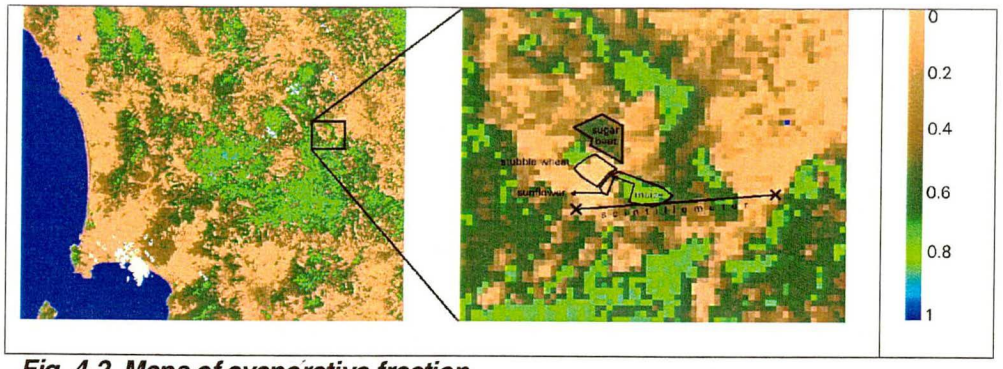

Fig. 4-2. Maps of evaporative fraction

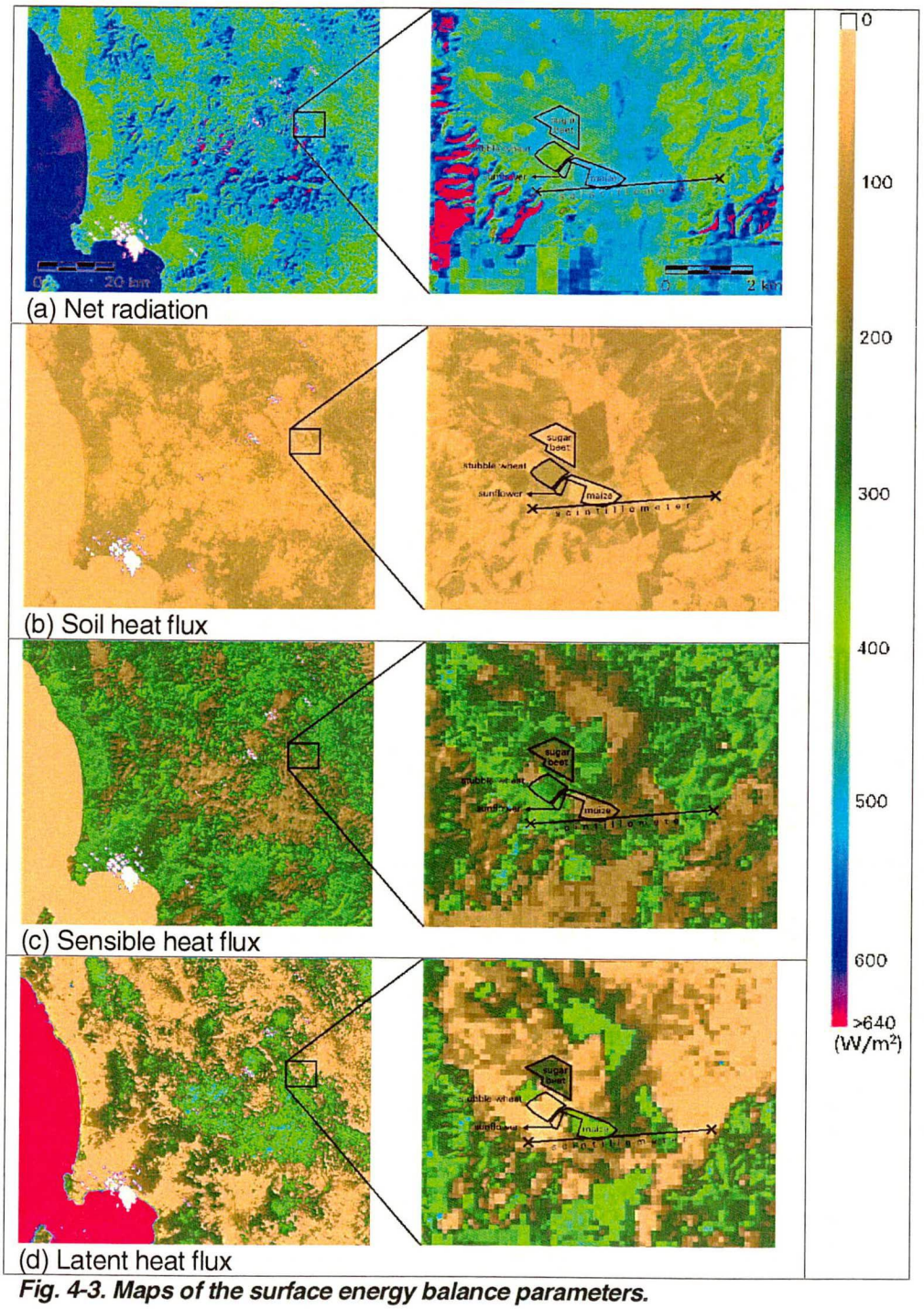

Fig. 4-3. Maps of the surface energy balance parameters.

Latent heat flux

The latent heat flux is the amount of energy used for the evaporation process of the soil and the transpiration process of the plants. It is calculated from the net available energy and the evaporative fraction as:

$$\lambda E = \Lambda(R_n - G_0) \tag{4-20}$$

Fig. 4-3(d) is the map of the latent heat flux.

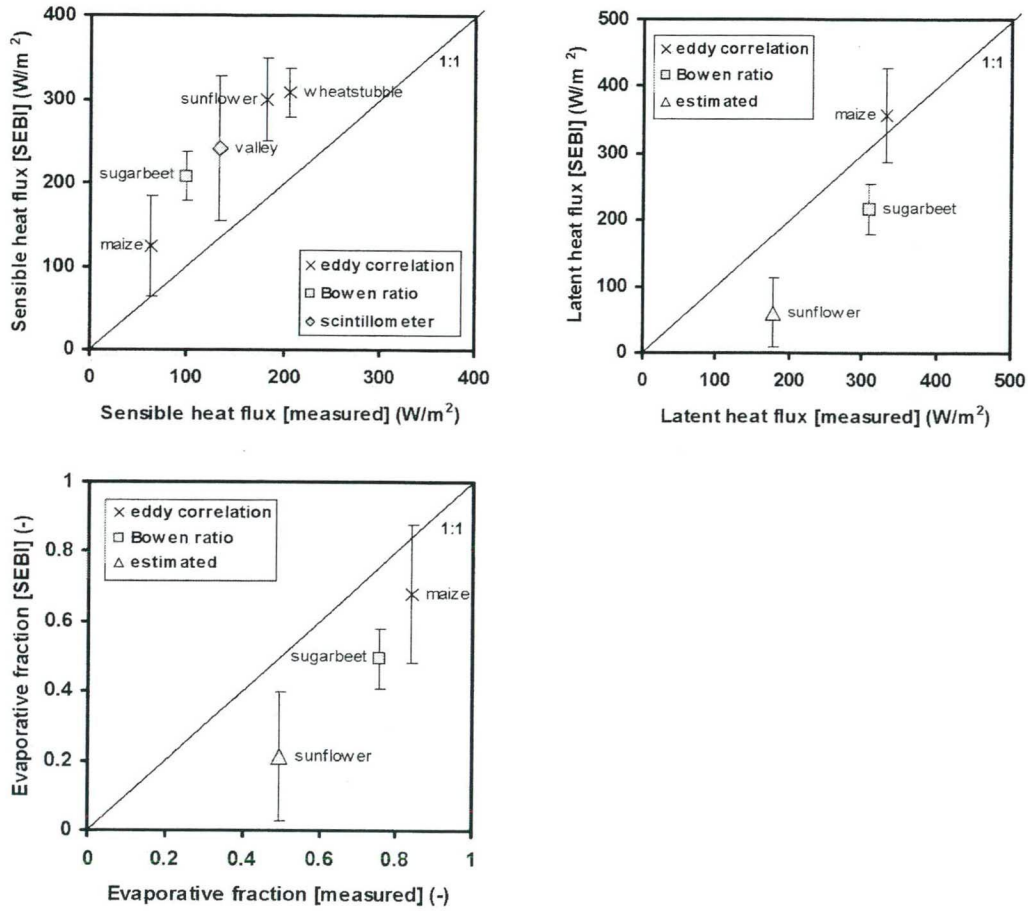

Fig. 4-4. Validation of the SEBS calculated results against the field measurements for the sensible heat flux, latent heat flux and evaporative fraction, together with the 1:1 line.

4.4 Validation

In Fig. 4-4 the SEBS results are plotted against the measured values in the field for the sensible and latent heat fluxes and the evaporative fraction. The 1:1 line is also plotted in the graphs. The SEBS values of the different field sites are the area-averaged values according to the field site boundaries in Fig. 4-1. No attention is paid to the calculation of a footprint for the sensible and latent heat flux, since the wind speed was very low (see Table 4-1). The field measurements of the sensible and latent heat flux values are the 30 minutes averaged values from 9:00-9:30 GMT, because some unexplained decreases occur for some fields during the next 30 minutes. For the scintillometer measurements the 5 minutes averaged value (9:25-9:30 GMT) is used.

The graph of sensible heat flux shows that the SEBS values are systematically too high. These systematically higher SEBS values can be explained by the fact that there exists also a similar difference in the net available energy measured in the field by radiation measuring devices and by devices, which measure turbulent heat fluxes. Another reason can be that this is a 5 minutes averaged value, while the other field measurements concern 30 minutes averaged values. Due to the heavily fluctuating flux measurements the 5 minutes averaged values can differ a lot from the 30 minutes averaged values.

The same problems as with the sensible heat flux occur for the latent heat flux. Therefore it is better to compare the evaporative fraction, which is independent of the magnitude of the different energy and radiation budget measurements. SEBS estimates underestimate the evaporative fraction compared to field measurements. The largest difference for the sunflower site is approximately 15%. However this is caused by using the net radiation from the radiation budget together with the eddy correlation measurement of sensible heat flux.

4.5 Conclusions

This case study to map the energy balance terms in Tuscany, Italy with Landsat TM data gave promising results. For the sensible heat flux the SEBS fluxes are estimated systematically too high. This is the result of the large discrepancies between the field measurements of the net available energy measured by radiation budget method and by energy budget devices.

Apart from possible inadequate parameterisations used in SEBS, two uncertainties are considered to contribute to the discrepancies between the SEBS estimates and in-situ measurements. The first factor is the determination of the values of the roughness length for momentum transfer. A higher roughness length (resulting in lower resistance) will cause a high sensible heat flux, when other factors remain unchanged. To estimate the roughness length of momentum transfer, a very simple method using a NDVI parameterisation is applied. The accuracy of the parameterisation has not been determined in this study. Another factor is the accuracy of the surface temperature. Only a very simple correction is applied in this study. Again its accuracy is uncertain. While a difference of 2 K can contribute to a difference of more than 40 Wm^{-2} for average conditions with resistances in the order of 50 sm^{-1}.

The sensible heat fluxes measured with the scintillometer instrument prove to be of good quality. Since the scintillometer measures the sensible heat flux over large distances (500 m – 3 km), it can be an ideal medium to validate the fluxes. Because the measured fluxes are already an averaged value over a large area, less attention needs to be paid to the fetch area of the flux measurement.

Since the SEBS estimates overestimate sensible heat fluxes as compared to available measurements in the field with an offset of approximately 100 Wm^{-2}, both of the above mentioned two factors must contribute to the same direction. Further investigation on these aspects is necessary before the present method can be routinely applied for estimation of regional evaporation. Nevertheless, it should be pointed out that the present method does not need any a priori knowledge of heat flux measurements, thus it is an independent method as such.

Acknowledgements

The authors would like to thank: (I) Ce.S.I.A. of the Accademia dei Georgofili, Florence, Italy, for the provision of the the Landsat TM scene and the DEM data; (ii) the Dept. of

Geography of the University of Basel, Switzerland, for the provision of the ground truth data at the maize, sugarbeet and sunflower sites; (iii) the University of Padova, Italy, for the provision of the ground truth data of the wheat stubble site and (iiii) the Dept. of Meteorology of the Wageningen University, the Netherlands, for the provision of the scintillometer flux measurements.

5 Estimation of evaporation using SEBS - NL

(C. Jacobs, G.J. Roerink, Z. Su)

Abstract
The Surface Energy Balance System (SEBS) (Su, 2000; Chapter 2) is applied in this contribution to three Landsat Thematic Mapper scenes of 1997 located in the Netherlands. Firstly a brief review is given to a set of necessary inputs for SEBS. These inputs include among others, surface albedo, vegetation indices, emissivity, temperature, roughness and incoming global radiation. Then these inputs are used to derive the evaporative fraction using SEBS. A preliminary comparison is performed between the derived evaporative fraction and limited in-situ point measurement data.

5.1 Introduction

In this contribution we will apply the SEBS to three Thematic Mapper (TM) scenes from 1997 for the Netherlands. Firstly a brief review is given to a set of necessary inputs for SEBS. These inputs include among others, surface albedo, vegetation indices, emissivity, temperature, roughness and incoming global radiation. Then these inputs are used to derive the evaporative fraction using SEBS. A preliminary comparison is performed between the derived evaporative fraction and limited in-situ point measurement data.

5.2 Data and study area

5.2.1 Description of study area

The study concentrated on test sites located in the center of the Netherlands.

The measurement tower 'Loobos' is located two kilometers south-west of Kootwijk on the Veluwe. In a radius of 500 meters 89% of the vegetation consists of pine trees, 3.5% is open vegetation e.g. heather and the rest is a mixture of coniferous and deciduous trees. The co-ordinates of the tower are 5° 44' 38" E and 52° 10' 00' N (figure 5-1). The 22 meter high measurement tower started its first observations in 1995 to study the water demands of forests on a regional scale (Elbers *et al.*, 1996).

Another measurement tower 'Fleditebos' is located approximately 5 kilometers west of Zeewolde in the Flevopolders. In a radius of 500 meters 93.5% of the vegetation consists of deciduous forest. The main forest type is poplar (76%) other forest species are ash (9.4%), oak (3.8%) and maple (3.0%) The co-ordinates of the tower are 5° 27' 12" E and 52° 19' 06' N (figure 5-1). The 24 meter high measurement tower also started its first observations in 1995 (Elbers *et al.*, 1996).

Figure 5-1 shows the CORINE land cover database[1] for the wider surroundings of the measurement sites.

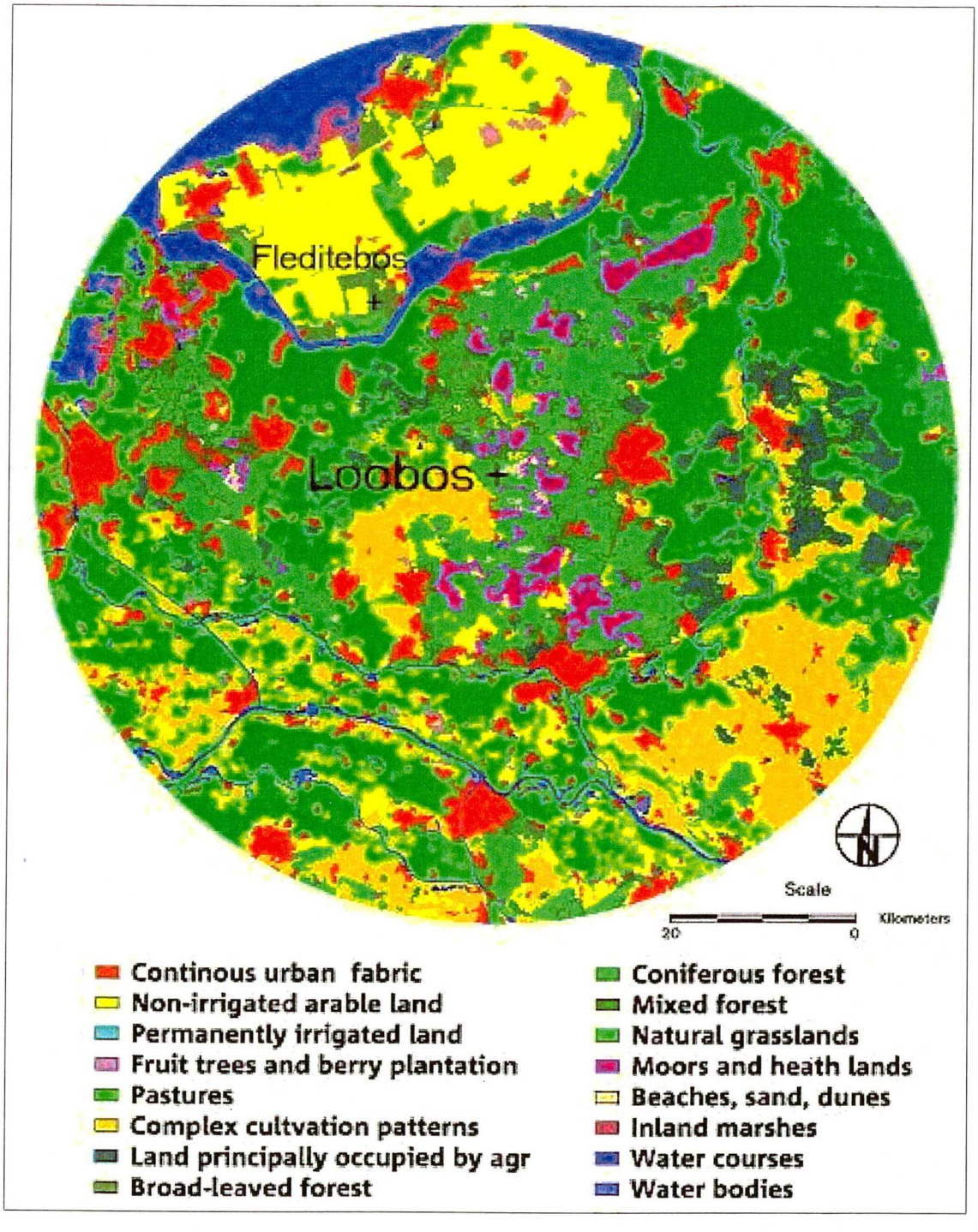

Figure 5-1 CORINE land cover database for a radius of 50 km around the measurement sites Loobos and Fleditebos, the Netherlands

[1] The CORINE land cover project is co-ordinated by the European Environmental Agency. The database is made by visual interpretation of high-resolution satellite images, e.g. Landsat TM and SPOT-XS, at a scale of 1 : 100 000, with simultaneous consultation of ancillary data (CEC 1993). The CORINE legend distinguishes 44 classes grouped in a hierarchical nomenclature and is landscape and ecology oriented.

5.2.3 Description of satellite data

Three Landsat Thematic Mapper 5 images for the Netherlands have been used (table 5-1). All images included the Loobos site, and the image of 10 March included the Fleditebos site.

Table 5-1 Landsat TM satellite images used for the study area in the Netherlands

Date TM image	Julian day	GMT	Local time	No. of rows	No of. columns
10 March 1997	69	10:00 AM	11:00 AM	4344	4644
7 June 1997	158	10:00 AM	12:00 AM	3947	2462
10 August 1997	222	10:00 AM	12:00 AM	3754	2340

5.2.4 Meteorological data

The meteorological data that were available for the Dutch study area were obtained from different meteorological stations (Loobos, Fleditebos, De Bilt) which made observations at hourly or half-hourly intervals. Loobos and Fleditebos are sites with specific instruments designed for research purposes, while De Bilt is equipped with standard meteorological instruments operated by the Dutch meteorological service (KNMI). Furthermore, atmospheric soundings were available for the days with a satellite overpass (De Bilt).

A few examples of the meteorological data which are relevant for use with remote sensing data are shown below.

Short-wave radiation components
The meteorological station at Loobos and Fleditebos carried out measurements of both the incoming and reflected short-wave radiation. Figure 5-2 illustrates the incoming and reflected short-wave radiation at Loobos on the 10th of August 1997.

Starting with sunrise at 4:30 GMT, the incoming short-wave radiation increases rapidly to a maximum of about 800 Wm^{-2} at 11:00 GMT. The incoming short-wave radiation then decreases with decreasing solar elevation until zero is reached with sunset at about 18:00 GMT. The reflected or outgoing solar radiation is small compared to the incoming solar radiation and never exceeds 100 Wm^{-2}.

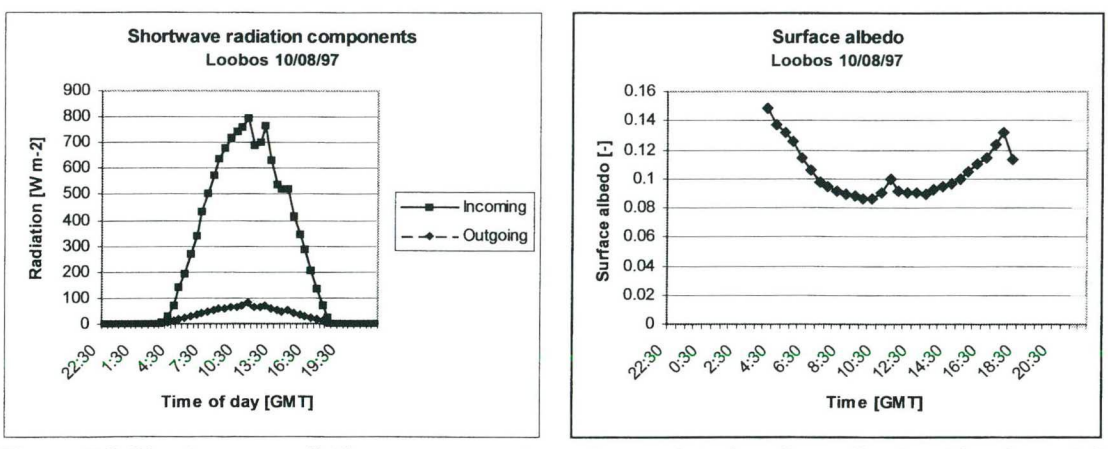

Figure 5-2 Short-wave radiation components and associated surface albedo at Loobos at 10 August 1997

The distinct hyperbolic shape of the surface albedo over the day demonstrates the surface albedo is not a fixed value but depends on the solar angle. At sunrise surface albedo values of about 0.15 are recorded which rapidly decrease until 8:30. The surface albedo then stabilises at values around 0.09 for the time-period between 8:30 and 14:30, and then rises again to about 0.14 at sunset.

The satellite overpass of Landsat TM is at 10:00 GMT and falls within the period that the surface albedo stabilises. The surface albedo values derived from Landsat TM can therefore be regarded as a good estimate of the 'true' surface albedo.

Long-wave radiation components
The second important parameter that was measured by the meteorological station is the emitted long-wave radiation, which is related to the temperature of the surface. Figure 5-3 illustrates the long-wave radiation flux for the 10th of August at the Loobos measuring site. The primary and secondary Y-axes are related to the long-wave radiation flux and corresponding surface temperature respectively.

The minimum surface temperature of 288 K (15 °C) at the 10th of August is reached just before sunrise, while the maximum surface temperature of 304 K (31 °C) corresponds roughly with the maximum of the incoming solar radiation. A distinct feature is also the almost linear decrease in surface temperature during the night. This effect is caused by the loss of energy at the surface due to continuous emission of long-wave radiation, which is not compensated by incoming short-wave radiation during night-time.

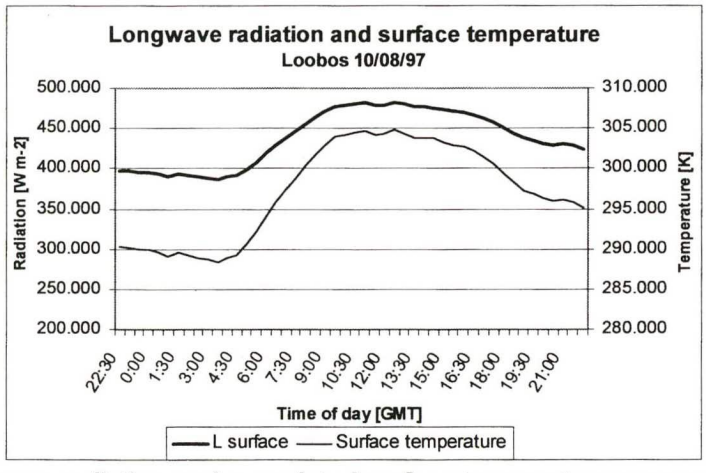

Figure 5-3 Longwave radiation and associated surface temperature measured at the Loobos site on10 August 1997

Fluxes of the surface energy balance
Figure 5-4 illustrates the daily paths of the energy fluxes at Loobos on the 10th of August. The net radiation is the overall amount of energy that is available and which is positive during day-time when solar radiation adds energy to the system and negative during night-time due to continuous emission of long-wave radiation by the surface. The soil heat flux is not shown in the figure, because this component is generally a small fraction of the net radiation.

The sensible and latent heat fluxes at the Loobos site are roughly equal to each other on the relevant day. The first 4 hours after sunrise, the sensible heat flux however lags behind the latent heat flux, until they are more or less equal at 9:00. This lag in energy flux has probably to do with the fact that plants can start photosynthesis as soon as there is

sunlight available and therefore the latent energy flux rises quickly. In the case of the sensible heat flux, a temperature gradient between the surface and the air has to build first before this energy flux can emerge. Also the effect of storage of energy in the canopy layer of the forest at the beginning of the day may play a role.

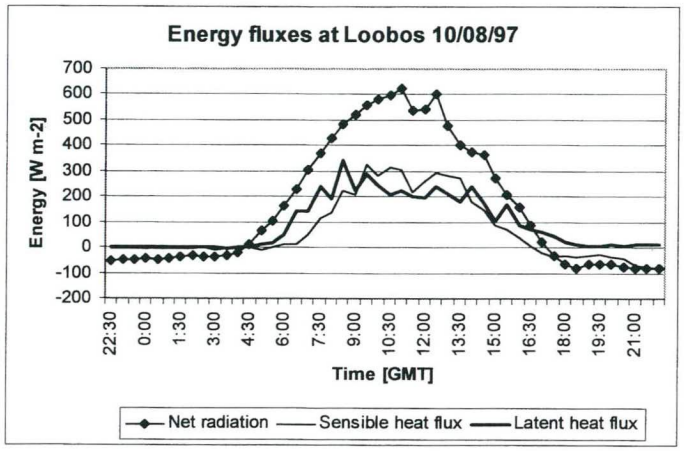

Figure 5-4 Energy fluxes in the surface energy balance at Loobos site on 10 August 1997

With regard to the satellite overpass time, it can be observed that the heat fluxes are more or less stabile at 9:00. Therefore the heat fluxes that are obtained from the meteorological station should be well comparable the with energy fluxes obtained from the satellite which overpasses the area at 10:00 GMT.

The Surface Energy Balance System applied to TM data

The details of the Surface Energy Balance System (SEBS) has been given by Su (this issue). We will only describe the specifications used in generating evaporative fractions using the TM data and radiosonde data.

Primary inputs to SEBS:

A. Remote sensing physical parameters derived from TM data
A1. albedo (-)
A2. potential surface temperature (K)
A3. Normalized Difference Vegetation Index (-)
A4. emissivity (-)
A5. LAI, vegetation fractional coverage and roughness length for momentum transfer

B. Radiosonde and Surface in-situ data
B1. clear sky downward shortwave radiation (W/m^2)
B2. clear sky downward longwave radiation (W/m^2)
B3. PBL-height (m)
B4. Surface pressure (Pa)
B5. PBL-averaged specific humidity (kg/m^3)
B6. PBL-averaged potential temperature (K)
B7. PBL-averaged horizontal wind speed (m/s)

The relevant parameters for this study are given in Table 5-2.

Table 5-2. Input parameters for application of SEBS to the TM data.

Parameter/Variable	10 March 1997	7 June 1997	10 August 1997
Surface temperature (^{0}C)	TM derivative	TM derivative	TM derivative
Surface albedo (-)	TM derivative	TM derivative	TM derivative
NDVI (-)	TM derivative	TM derivative	TM derivative
Roughness height for momentum transfer (m)	Literature values based on land use classification	Literature values based on land use classification	Literature values based on land use classification
PBL Depth (m)	312.0	1500.0	2670.0
PBL pressure (Pa)	99400.0	84800.0	74100.0
PBL potential temperature (K)	287.22	299.6	303.45
PBL specific humidity (kg/kg)	0.00661	0.02218	0.02461
PBL wind speed (m/s)	3.0	8.0	7.0
Surface pressure (Pa)	103200.0	100800.0	102000.0
Downward long-wave radiation (W/m^2)	275.0	384.1	384.0
Surface short-wave clear sky radiation (W/m^2)	449.0	783.5	715.0

Table 5-3 Constants for conversion of DN to spectral radiance (source: EOSat technical Notes, 1993, Markham and Barker, 1987)

Thematic mapper	gain [mW cm^{-2} sr^{-1}]	bias [mW cm^{-2} sr^{-1}]	Bandwidth [μm]
Channel 1	0.0042	-0.0169	0.066
Channel 2	0.0104	-0.0418	0.082
Channel 3	0.0066	-0.0262	0.067
Channel 4	0.0118	-0.0593	0.128
Channel 5	0.0028	-0.0165	0.217
Channel 7	0.0017	-0.0085	0.252

5.3 Results and discussions

We will now describe the methods to derive from remotely observables to the input parameters to SEBS.

5.3.1 Input parameters SEBS

Surface albedo

The surface albedo can be obtained from the TM channels in the visible, near-infrared and mid-infrared parts of the electromagnetic spectrum. The satellite data, which consist of digital numbers have to be converted into radiance values using a linear relationship (Eq. 5-1). The constants for this relationship are given in Table 5-3.

$$L_x = \frac{(bias_x + gain_x \cdot DN)}{bandwidth_x} \qquad (5\text{-}1)$$

Where

L_x = Spectral radiance for TM channel X [mW cm^{-2} sr^{-1} μm^{-1}]

$bias_X$, $gain_X$ = Channel-specific minimum and maximum spectral radiances [mW cm^{-2} sr^{-1}]
DN = Digital number
$bandwidth_x$ = Bandwidth of the relevant TM channel [μm]

When the spectral radiance is known for each TM channel, the surface reflectance for each channel can be calculated, taking into account the geometrical solar parameters:

$$r_X = \frac{\pi L(X) d_s^2}{K^{\downarrow}(X)\cos\theta} \qquad (5\text{-}2)$$

Where
r_X = In-band planetary reflectance for channel X [-]
d_s^2 = Relative sun-earth distance [-]
$K^{\downarrow}(X)$ = Mean solar exo-atmospheric irradiance in channel X [mW cm^{-2} μm^{-1}] table 5-4)
θ = Solar zenith angle [rad]

Table 5-4 Solar exo-atmospheric spectral irradiances for the relevant TM channels and associated weight factors

Thematic mapper	Solar exo-atmospheric spectral irradiance [mW cm^{-2} μm^{-1}]	Weight factor
Channel 1	195.7	0.293
Channel 2	182.9	0.274
Channel 3	155.7	0.233
Channel 4	104.7	0.157
Channel 5	21.93	0.033
Channel 7	7.452	0.011

The albedo values that have been derived are planetary albedo values which have to be corrected for atmospheric influences. A correction procedure has been used (Koepke, 1985) which defines the surface albedo as:

$$r_0 = \frac{r_p - r_a}{\tau^2} \qquad (5\text{-}3)$$

Where
r_0 = Surface albedo [-]
r_p = Planetary albedo [-]
r_a = Apparent atmospheric albedo [-]
τ = One-way atmospheric transmissivity [-]

Values for τ can be obtained using:

$$\tau = \frac{K^{\downarrow}}{K^{TOA}} \qquad (5\text{-}4)$$

Where $K^{\downarrow}$ is taken from the meteorological observations at the time of satellite overpass and K^{TOA} is the solar radiation intensity that can be expected at the top of the atmosphere as a function of the Julian day and overpass time. The atmospheric albedo (r_a) has been

determined by solving equation 3 for the Loobos site for which the values of r_0 and r_p are known. The surface albedo at the Loobos site was determined as the ratio of $K^{\uparrow}$ over $K^{\downarrow}$ and the planetary albedo was taken from the TM images. Table 5-5 shows the values of τ and r_a that have been obtained for the Netherlands. The atmospheric transmissivity was calculated as the average transmissivity at the four meteorological stations.

Table 5-5 Atmospheric properties used to correct the satellite obtained planetary albedo

Date of TM image	Atmospheric transmissivity (τ) [-]	Apparent atmospheric albedo (r_a) [-]
Netherlands		
10 March 1997	0.660	0.0242
7 June 1997	0.726	0.0364
10 August 1997	0.725	0.0413

Vegetation index

The normalized difference vegetation index (NDVI) is used, which can be calculated as

$$NDVI = \frac{r_{nir} - r_{red}}{r_{nir} + r_{red}} \qquad (5\text{-}5)$$

Where r_{nir} and r_{red} are the reflectances in the near-infrared and red satellite channels. The NDVI was calculated using the planetary reflectances in TM channels 3 and 4. No atmospheric correction was applied to the NDVI as no field measurements in the specific channels were available.

NDVI maps are shown in figure 5-5.

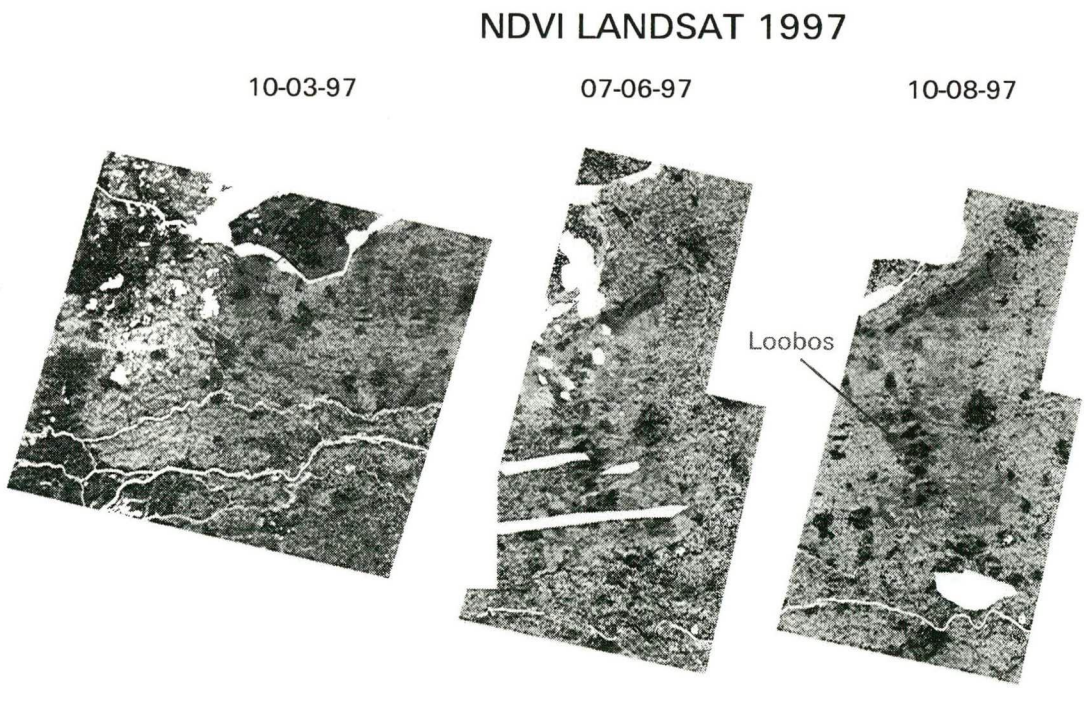

Figure 5-5 Landsat 1997 NDVI maps

Surface emissivity

The relationship proposed by Van de Griend and Owe (1993) is used; this reads

$$\varepsilon_0 = 1.009 + 0.047 \ln(NDVI) \tag{5-6}$$

which is valid for NDVI=0.16-0.74. This equation is empirical and is valid only for the conditions under which the measurements have been made.

Surface temperature

At the Loobos site both the incoming ($L^{\downarrow}$) and outgoing ($L^{\uparrow}$) longwave fluxes were measured and therefore the surface temperature can be derived. The broadband long-wave radiative flux emitted at the Loobos site can be calculated and the surface temperature T_O can be subsequently be derived using:

$$L_{surface} = L^{\uparrow} - (1-\varepsilon_0)L^{\downarrow} \tag{5-7}$$

$$T_0 = \sqrt[4]{\frac{L_{surface}}{\varepsilon_0 \sigma}} \tag{5-8}$$

Next, the amount of radiation emitted by the Loobos site within the spectral range of the TM6 sensor can be calculated by numerical integration of Planck's law over the 10.4–12.5 µm interval:

$$L(TM6)_{surface} = \varepsilon_{TM6} \sum_{10.4}^{12.5} L_\lambda(T_0) \tag{5-9}$$

$$L_\lambda(T_0) = \varepsilon_\lambda \frac{3.74 \cdot 10^8}{\lambda^5} \left[\exp\left(\frac{1.44 \cdot 10^4}{\lambda T_0}\right) - 1 \right]^{-1} \tag{5-10}$$

The radiation at the top of the atmosphere ($L(TM6)_{TOA}$) can be derived from the satellite imagery by taking the DN value in channel 6 for the Loobos site and applying (Markham and Barker, 1987):

$$L(TM6)_{TOA} = 0.1238 + \frac{1.560 - 0.1238}{255} DN \tag{5-11}$$

The value obtained for $L(TM6)_{TOA}$ however has to be converted to Wm^{-2} by multiplying with 10, π and the bandwidth of the sensor of 2.1 µm. The ratio between $L(TM6)_{TOA}$ and $L(TM6)_{surface}$ can now be determined and is assumed to be constant for the entire image. The long-wave radiation at the top of the atmosphere for each pixel can now be converted into a surface emittance using this ratio.

Because Eq. (5-7) can only be applied to derive long-wave radiation from surface temperature, it is not possible to invert the equation and calculate the surface temperatures directly. The long-wave radiation for a number of surface temperatures can however be calculated and simple linear regression can be used to relate radiation to surface temperature. Although the relation between surface temperature and emission of radiation is basically non-linear, it can be approximated by a linear relationship for the 280–330 K range with an R^2 of greater than 0.99. The correction factors used to correct the TM images of the Netherlands (Table 5-6) show a decreasing trend. The origin of this trend is not understood, but could be related to the fact that the difference between the

surface temperature and the air temperature near the surface becomes subsequently larger and therefore a larger correction is needed.

Table 5-6 Correction factors used to correct the long-wave radiation received by the Landsat TM satellite.

Date of TM image (Netherlands)	$L(TM6)_{TOA}/ L(TM6)_{surface}$ [-]
10 March 1997	0.9873
7 June 1997	0.9809
10 August 1997	0.9602

LAI, vegetation fractional coverage and roughness length for momentum transfer

Here we use a simple formula synthesized from Su (1996, 2000) to derive the leaf area index (LAI), since more accurate formulas are not available for the time being:

$$LAI = \left(NDVI \cdot \frac{1 + NDVI}{1 - NDVI + \delta NDVI} \right)^{1/2} \tag{5-12}$$

This formula is strictly only good for low vegetation since NDVI saturates at higher LAI values. However, there is not sufficient information in this study to support more sophisticated formulations.

The fractional vegetation coverage is calculated as follows:

$$f_c = \left(\frac{NDVI - NDVI_{\min}}{NDVI_{\max} - NDVI_{\min}} \right) \tag{5-13}$$

where $NDVI_{\min}$ is the NDVI for bare soil and $NDVI_{\max}$ for full vegetation coverage.

Literature values for roughness heights for momentum transfer are used (e.g. Wieringa, 1993) based on a land use classification. The values are the same for all three dates. This is certainly an over-simplification since it is known that the roughness length for momentum is influenced not only by the land use but also by actual leaf area index that changes seasonally. However the purpose of this study is to demonstrate that SEBS can be used with limited data, therefore we will not dwell into the details of different parameters.

A conversion is performed according to Brutsaert (1982) to derive vegetation height and displacement height for a given aerodynamic roughness height.

$$h = \frac{z_{0m}}{0.136} \tag{5-14}$$

$$d = \frac{2}{3} h \tag{5-15}$$

Some constants for vegetation are given as follows: C_d = 0.2, the canopy drag coefficient; C_t = 0.01, the leaf heat transfer coefficient; D_l = 0.05 (m), the leaf width.

5.3.2 Evaporative fractions

Having prepared the required inputs and parameters, the following steps are followed to derive the pixelwise evaporative fractions.

Firstly, the model of Su *et al.* (2000) is used to derive the roughness height for heat transfer. Then the Bulk Atmospheric Similarity (BAS) is used to derive the friction velocity, the sensible heat flux and the Obukhov length. Finally, the SEBI option within SEBS is used to calculate the pixelwise evaporative fractions.

The results are shown below in figure 5-6. The corresponding histograms are shown in figure 5-7.

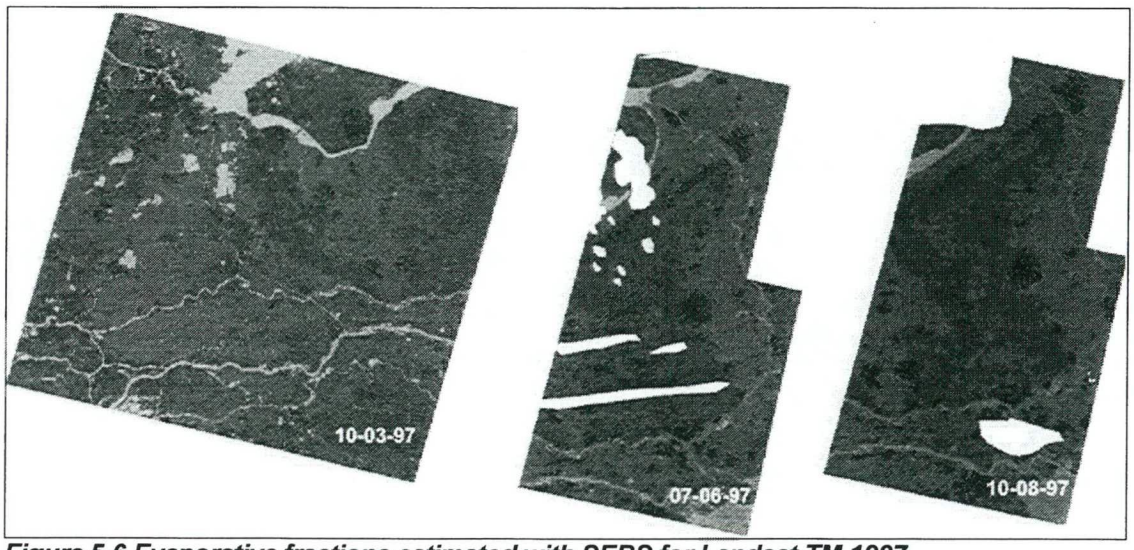

Figure 5-6 Evaporative fractions estimated with SEBS for Landsat TM 1997

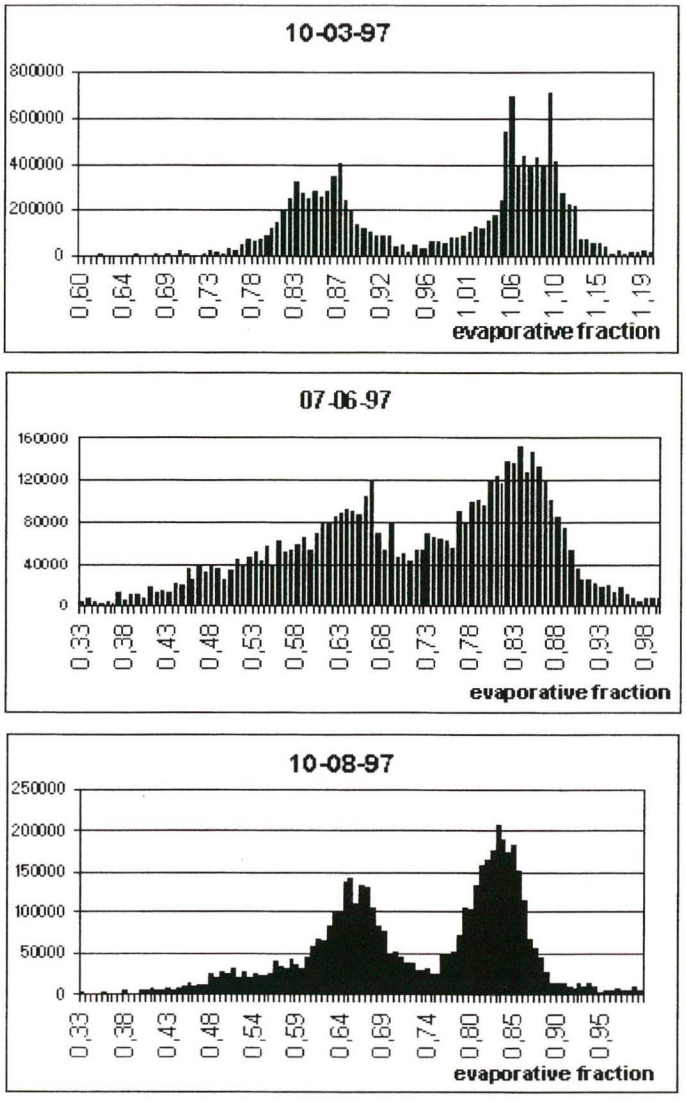

Figure 5-7 Histograms of the evaporative fractions

5.3.2 Comparison SEBS results to field measurements

To preliminary validate the derived evaporative fractions, the results have been compared with the evaporative fractions derived with the flux measurements (flux tower) from Loobos. For the 10th of March 1997 the field measurements at Loobos failed during satellite overpass. For this date, the results have been compared to measurements from Fleditebos. The results are shown in table 5-5.

Table 5-5 Comparison of the remotely sensed fluxes with field measurements for the study area. Satellite derived fluxes are means for a radius of 270 m (23 ha).

	Dates	Λ (-)	
		Field	Satellite
Loobos			
	10-03-97	-	0.88
	07-06-97	0.33	0.60
	10-08-97	0.46	0.61
Fleditebos			
	10-03-97	0.33	0.82

5.4 Discussions and conclusions

In this study, we have developed a set of methods for deriving land surface parameters. The SEBS is applied to three TM scenes in combination with PBL information from radiosonde data in the Netherlands.

The results indicate that:

-For all images, evaporative fraction values are systematically overestimated. For 7 June and 10 August, the results are still within physical limits (0-1), but for 10 March, more than half of the pixels has a value higher than 1.

-Two peaks appear in the evaporative fractions histogram functions: one peak represents forest (lower Λ values) and the other peak non-forest (higher Λ values). Forest has higher surface roughness values (than e.g. grassland, cereals or natural vegetation) which cause more turbulence and thus a larger sensible heat flux.

Since the same procedures are applied to the three data sets, the difference in the SEBS may be attributed to the uncertainties in the input parameters. As a matter of fact, the atmosphere is assumed uniform which may not be the case for all the three dates, since it is known that the Dutch weather changes rather rapidly from place to place. The simple atmospheric corrections applied to the images may not be adequate. There is no atmospheric correction applied when calculating the NDVI, which in turn was used to calculate the emissivity and the fractional vegetation coverage. This will certainly introduce errors. Additionally, the formulas used to calculate emissivity, LAI are all only valid for low vegetation, comparison of results obtained with these formulas for forest should only be regarded as indicative.

There is essentially hardly any atmospheric correction applied to derive the surface temperatures. The derivation of the surface temperature is based on regression with a few surface measurements. Since the measurements are done with radiometers with limited field of view and certainly can not cover the spatial resolution of the TM TIR sensor (120m), the representativeness of these measurements is not established. This may contribute to the major uncertainties in the derived evaporative fractions.

One particular case is worth of mentioning. The pixels representing roads have all too high Λ values due to the following reasons. The input T_0 file contains temperature values aggregated to 120 m pixels. This means that road pixels do not have the actual road temperature (should be usually higher than surroundings), but have been given the average temperature of the surrounding pixels (grass), i.e. the temperatures are lower than they actually should be. Such low temperatures with corresponding low roughness values result in the same circumstances as for water. Only higher resolution data (at most with pixel size half of the road width) will be able to resolve this problem.

In the present study we have not been able to investigate the details of the input parameters due to time constraints. It is expected that such analysis will reveal valuable information as regards to the necessary accuracy in the derived input data. As well as the accuracy in the derived final evaporative fractions.

6 Conclusions and overview of future work

(Z. Su)

This is a progress report for the project "ENVISAT - Actual Evaporation: Evaluation of algorithms to estimate actual evaporation of land surfaces with AATSR and MERIS observations", BCRS: 4.2/AP-13.

The general objective of the project is to evaluate selected algorithms to estimate actual evaporation using radiances observed with imaging radiometers in the visible to thermal infrared spectral region.

6.1 Conclusions

A brief description of the Surface Energy Balance System (SEBS) is given for the estimation of atmospheric turbulent fluxes and surface evaporation using satellite earth observation data in the visible, near infra-red, and thermal infrared frequency range (Chapter 2).

SEBS consists of the following components:
1. Preprocessing to derive land surface physical parameters, such as albedo, emissivity, temperature, vegetation coverage etc. from spectral reflectance and radiance measurements;
2. A model for the determination of the roughness length for heat transfer (Su et al. 2000);
3. The BAS (Bulk Atmospheric Similarity) theory for determination of friction velocity, sensible heat flux and the Obukhov stability length (Brutsaert, 1999)
4. The SEBI (Surface Energy Balance Index) concept for determination of evaporative fraction (Menenti & Choudhury, 1993).
Consequently, SEBS is applied to several site in Europe (Spain, Italy and the Netherlands) with different climates and land surface conditions.

In Chapter 3, we have developed a set of methods for deriving land surface parameters. The SEBS is applied to a TMS scene in combination with PBL information from radiosonde data for the Barrax area, Spain. The SEBS estimates of the evaporative fractions are confined between 0 and 1. In the Barrax area, there is a clear distinction between irrigated crops and non irrigated/fallow/bare parts. Two clear peaks appear in the histogram: one peak around $\Lambda = 0.25$ (fallow) and a smaller one around $\Lambda = 0.70$ (irrigated crops). Furthermore, looking at the pivot circles and the corresponding Λ values, the efficiency of the irrigation can be inferred.

The comparison of the SEBS estimates to field measurements is satisfactory. The relatively small differences can be explained by the differences in measurement heights, the fetch areas and method of measurement. Further, since the SEBS estimates are instantaneous values based on the remote sensing data, while the in-situ measurements are half-hourly averages, difference should also occur due to the turbulent nature of the heat fluxes. In the present study we have not been able to investigate the details of the quality of the input due to time constraints. Although various studies have used the TMS for various purposes (Bastiaanssen, 1995; Su *et al.*, 2000, Pelgrum, 2000) and the data

should be of good quality in terms of calibration and various corrections, some of the secondary inputs have to be derived using rather limited knowledge of the surface conditions and of actual physical relationships. It is expected that such analysis will reveal valuable information as regards to the necessary accuracy in the derived input data.

In Chapter 4, SEBS is applied to a Landsat scene for the Tuscany area, Italy. The results are promising. For the sensible heat flux the SEBS fluxes are estimated systematically too high. This is the result of the large discrepancies between the field measurements of the net available energy measured by the radiation budget method and by energy budget devices. Apart from possible inadequate parameterisations used in SEBS, two uncertainties are considered to contribute to the discrepancies between the SEBS estimates and in-situ measurements. The first factor is the determination of the values of the roughness length for momentum transfer. A higher roughness length (resulting in lower resistance) will cause a high sensible heat flux, when other factors remain unchanged. To estimate the roughness length of momentum transfer, a very simple method using a NDVI parameterisation is applied. The accuracy of the parameterisation has not been determined in this study. Another factor is the accuracy of the surface temperature. Only a very simple correction is applied in this study. Again its accuracy is uncertain. While a difference of 2 K can contribute to a difference of more than 40 Wm^{-2} for average conditions with resistances in the order of 50 sm^{-1}. Since the SEBS estimates overestimate sensible heat fluxes as compared to available measurements in the field with a offset of approximately 100 Wm^{-2}, both of the above mentioned two factors must contribute to the same direction. Further investigation on these aspects is necessary before the present method can be routinely applied for estimation of regional evaporation.

In Chapter 5, we have developed a set of methods for deriving land surface parameters. The SEBS is applied to three TM scenes in combination with PBL information from radiosonde data in the Netherlands. The results indicate that:
-For all images, evaporative fraction values are systematically overestimated. For 7 June and 10 August, the results are still within physical limits (0-1), but for 10 March, more than half of the pixels has a value higher than 1.
-Two peaks appear in the evaporative fractions histogram functions: one peak represents forest (lower Λ values) and the other peak non-forest (higher Λ values). Forest has higher surface roughness values (than e.g. grassland, cereals or natural vegetation) which cause more turbulence and thus a larger sensible heat flux.

Since the same procedures are applied to the three data sets, the difference in the SEBS may be attributed to the uncertainties in the input parameters. As a matter of fact, the atmosphere is assumed uniform which may not be the case for all the three dates, since it is known that the Dutch weather changes rather rapidly from place to place. The simple atmospheric corrections applied to the images may not be adequate. There is no atmospheric correction applied when calculating the NDVI, which in turn was used to calculate the emissivity and the fractional vegetation coverage. This will certainly introduce errors. Additionally, the formulas used to calculate emissivity, LAI are all only valid for low vegetation, comparison of results obtained with these formulas for forest should only be regarded as indicative. There is essentially hardly any atmospheric correction applied to derive the surface temperatures. The derivation of the surface temperature is based on regression with a few surface measurements. Since the measurements are done with radiometers with limited field of view and certainly can not cover the spatial resolution of the TM TIR sensor (120m), the representativeness of these measurements is not established. This may contribute to the major uncertainties in the derived evaporative fractions. In the present study we have not been able to investigate the details of the input parameters due to time constraints. It is expected that such

analysis will reveal valuable information as regards to the necessary accuracy in the derived input data. As well as the accuracy in the derived final evaporative fractions.

Finally, it should be pointed out that the application of SEBS does not require any a priori knowledge of the actual turbulent heat fluxes. We have just derived the necessary input data from the remote sensing data, the radiosonde data and in-situ data and applied them to SEBS. This indicates SEBS is a credible and independent approach.

Based on the case studies, the SEBS has been partially validated. Since the current project is limited by its available finance and time constraint (circa 15% of necessary finance), we have just focused to demonstrate the utility of SEBS for different climate and land surface conditions. No attempt has been made to refine the different procedures in order to improve the input data and the consequently the model estimates. Further effort is required to consolidate the findings in future projects.

6.2 Overview of future work

In the present phase of the project, it has not been possible to evaluate the additional values of the new spectral, directional and spatial features of the ENVISAT sensors since the data are not yet available during the project execution. However, it can be confidently expected that the new features will enable more accurate determination of the physical parameters (albedo, leaf area index, fractional coverage of vegetation, emissivity, and component temperatures) that are necessary for estimation of evaporation. Furthermore, if the evaporation and transpiration can be easily separated by using component temperatures that can be derived from the (A)ATSR sensors, the carbon exchanges between the land surface and the atmosphere can also be determined. This latter aspect will be a major progress in characterising the spatial distributions of the sources and sinks of the carbon fluxes. At the present, only indirect methods based on point measurements and up-scaling or based on estimating of the maximum assimilation possibilities of carbon are available.

At present, a first initiative has been undertaken to investigate the possibility of applying the techniques developed in the project to the policy making processes of the Ministry of the Agriculture, Nature Conservation and Fisheries (LNV). A seminar has been organized to identify the parameters and variables that are needed in the models used by the Nature Planning Office (NPB). A project under the GIS/RS programme of LNV has also been started to demonstrate the feasibility of applying more physical measurements in the NPB models. To this purpose, the Surface Energy Balance System (SEBS) developed in this project will be applied to make a time series of evaporation and soil moisture. This will in turn be used to validate if the NPB models' outputs can capture the spatial distribution of these variables. In the future, direct assimilation of the remote sensing information in the NPB models will be investigated.

References

Bastiaanssen, W.G.M., 1995. Regionalization of surface flux densities and moisture indicators in composite terrain. Ph.D. Thesis, Wageningen Agricultural University (appeared also as Report 109, DLO-Winand Staring centre), Wageningen, The Netherlands: 273 p.

Bolle, H.-J., André, J.C., Arrue, J.L., Barth, H.K., Bessemoulin, P., Brasa, A., de Bruin, H.A.R., Cruces, J., Dugdale, G., Engman, E.T., Evans, D.L., Fantechi, R., Fiedler, F., van de Griend, A., Imeson, A.C., Jochum, A., Kabat, P., Kratzsch, T., Lagouarde, J.-P., Langer, I., Llamas, R., Lopez-Baeza, E., Melia Miralles, J., Muniosguren, L.S., Nerry, F., Noilhan, J., Oliver, H.R., Roth, R., Saatchi, S.S., Sanchez Diaz, J., de Santa Olalla, M., Shuttleworth, W.J., Sogaard, H., Stricker, H., Thornes, J., Vauclin, M., Wickland, D., 1993. EFEDA: European field experiments in a desertification-threatened area, Ann. Geophys., 11, 173-189.

Bosveld, F.C., 1999: Exchange processes between a coniferous forest and the atmosphere. Ph.D. dissertation, Wageningen Agricultural University, 181pp. (ISBN 90-5808-111-7).

Brest, C.L. & S.N. Goward, 1987. Deriving surface albedo measurements from narrow band satellite data, Int. J. Remote Sensing 8 (3): 351-367.

Bruin, H.A.R. de, B.J.J.M. van den Hurk and W. Kohsiek, 1995. The scintillation method tested over a dry vineyard area. Boundary-Layer Meteorology 76: 25-4.

Brutsaert, W., 1982. Evaporation into the atmosphere, Reidel, Dordrecht, 299 pp.

Brutsaert, W., 1998: Land-surface water vapor and sensible heat flux: Spatial variability, homogeneity, and measurement scales. Water Resour. Res., 34, 2433-2442.

Brutsaert, W., 1999: Aspects of bulk atmospheric boundary layer similarity under free-convective conditions. Rev. Geophy., 37, 439-451.

CEC (1993). CORINE Land Cover technical guide. European Union. Directorate-General Environment, Nuclear Safety and Civil Protection. Luxemburg. ISBN 92-826-2578-8.

Choudhury, B.J., and J.L. Monteith, 1988: A four layer model for the heat budget of homogeneous land surfaces. Q.J.R. Meteorol. Soc., 114, 373-398.

Daughtry, C.S.T., W.P. Kustas, M.S. Moran, P.J. Pinter, R.D. Jackson, P.W. Brown, W.D. Nichols and L.W. Gay, 1990. Spectral estimates of net radiation and soil heat flux. Rem. Sens. Of Env. 32: 111-124.

Elbers, J.A., Dolman, A.J., Moors, E.J. and Snijders, W., 1996. Hydrologie en waterhuishouding van bosgebieden in Nederland. Fase 2: Meetopzet en eerste resultaten. Rapport 333.2, DLO-Winand Staring Centre, Wageningen, the Netherlands.

EOSAT Tech. Note, 1986. New look-up tables, No. 1, 7pp.

EOSAT, 1993. Fast Format Document for TM Digital products. Version B, effective December 1, 1993.

Iqbal, M., 1983. Introduction to solar radiation. Academic Press, 390 pp.

Jackson, R.D., S.B. Idso, R.J. Reginato, and P.J. Pinter Jr., 1981: Canopy temperature as a crop water stress indicator. Water Resour. Res., 17(4), 1133-1138.

Jackson, R.D., W.P. Kustas, and B.J. Choudhury , 1988: A re-examination of the crop water stress index. Irrig. Sci., 9, 309-317.

Kustas, W.P., and C.S.T. Daughtry, 1989c: Estimation of the soil heat flux/net radiation ratio from spectral data. Agric. For. Meteorol., 49, 205-223.

Li, Z.-L., M.P. Stoll, R. Zhang, L. Jia and Z. Su, 2000: On the separate retrieval of soil and vegetation temperatures from ATSR data. Science in China (in press).

Markham, B.L. and Barker, J.B., 1987, Thematic Mapper bandpass solar exo-atmospherical irradiances. Int. J. Remote Sensing 8(3):517-523.

Massman, W.J., 1997: An analytical one-dimensional model of momentum transfer by vegetation of arbitrary structure. Boundary-Layer Meteorol., 83, 407-421.

Massman, W.J., 1999: Molecular diffusivities of Hg vapor in air, O_2 And N_2 near STP and the kinematic viscosity and the thermal diffusivity of air near STP. Atmos. Environ., 33, 453-457.

Menenti, M. 1984. Physical aspects of and determination of evaporation in deserts applying remote sensing techniques. Report 10 (special issue), Institute for Land and Water Management Research (ICW), The Netherlands, 202pp.

Menenti, M. and B.J. Choudhury, 1993. Parameterization of land surface evaporation by means of location dependent potential evaporation and surface temperature range. Proceedings of IAHS conference on Land Surface Processes, IAHS Publ. 212: 561-568.

Menenti, M., Bastiaanssen, W.G.M., van Eick, D. and Abd el Karim, M.H., 1989. Linear relationships between surface reflectance and temperature and their application to map actual evaporation of groundwater, Adv. Space Res., 9, 165-176.

Monteith, J.L., 1973: Principles of environmental physics. Edward Arnold Press, 241 pp.

Pelgrum, H., 2000: Spatial aggregation of land surface characteristics – impact of resolution of remote sensing data on land surface modelling. Ph.D. thesis, Wageningen University,151 pp.

Press, W.H., S.A. Teukolsky, W.T. Vetterling, and B.P. Flannery, 1997: Numerical Recipes in C: The Art of Scientific Computing. Cambridge Univ. Press, 994pp.

Roerink, G.J., Z. Su, M. Menenti, 2000, S-SEBI: A simple remote sensing algorithm to estimate the surface energy balance. Physics and Chemistry of the Earth, 25, 147-157.

Stanghellini, C., 1987, Transpiration of greenhouse crops – an aid to climate management, Ph.D thesis, Agriculture University,Wageningen, The Netherlands.

Su, Z., 1996, Remote sensing applied to hydrology: the Sauer River Basin study, Ph.D. Dissertation, Heft 15, Schriftenreihe Hydrologie/Wasserwirtschaft, Faculty of Civil Engineering, Ruhr University Bochum, Germany, pp. 199.

Su, Z., 2000, Remote sensing of land use and vegetation for mesoscale hydrological studies, Int. J. Remote Sensing, 21, 213-233.

Su, Z., 2001: A Surface Energy Balance System (SEBS) for estimation of turbulent heat fluxes from point to continental scale. In Su and Jacobs (eds), Advanced Earth Observation – Land Surface Climate, BCRS report (in press).

Su, Z., H. Pelgrum, M. Menenti, 1999, Aggregation effects of surface heterogeneity in land surface processes, Hydrology and Earth System Sciences. 3(4), 549-563.

Su, Z., P.A. Troch, and F.P. de Troch, 1997: Remote sensing of bare surface soil moisture using EMAC/ESAR data. Int. J. Remote Sens., 18, 2105-2124.

Su, Z., T. Schmugge, W.P. Kustas, W.J. Massman, 2000: An evaluation of two models for estimation of the roughness height for heat transfer between the land surface and the atmosphere. J. Appl. Meteorology (in review).

Valor and Caselles, 1996. Mapping land surface emissivity from NDVI: application to European, African, and South American areas. Remote Sens. Environ. 57: 167-184.

Van de Griend A.A. and Owe, M., 1993. On the relationship between thermal emissivity and the normalized difference vegetation index for natural surfaces. Int. J. Rem. Sens. 14, 1119-1131.

Van den Hurk, B.J.J.M & Z. Su 1999: Chapter 6.1, Heat and Mass Transfer, in M. Menenti (ed.) Requirements to a Hyper-Spectral and Directional Land-Surface Processes and Interactions Remote Sensing Mission. Final report, ESA.

Verhoef, W., 1998: Theory of radiative transfer models applied in optical remote sensing of vegetation canopies. Ph.D. dissertation, Wageningen Agricultural University, 310pp. (ISBN 90-5485-804-4).

Verhoef, A., H.A.R. de Bruin, and B.J.J.M. van den Hurk, 1997: Some practical notes on the parameter for sparse vegetation. J. Appl. Meteorol., 36, 560-572.

Wieringa, J. 1986: Roughness-dependent geographical interpolation of surface wind speed averages. Q.J.R. Meteor. Soc. 112, 867-889.

Wieringa, J. 1993: Representative roughness parameters for homogeneous terrain. Boundary Layer Met. 63,323-363.

List of acronyms and abbreviations

ATSR	Along Track Scanning Radiometer
AATSR	Advanced Along Track Scanning Radiometer
AVHRR	Advanced Very High Resolution Radiometer
BATS	Biosphere Atmosphere Transfer Scheme
BRDF	Bidirectional Reflectance Distribution Function
DEM	Digital Elevation Model
DWT	Discrete Wavelet Transform
EFEDA	ECHIVAL Field Experiment in Desertification Threatened Areas
EOS	Earth Observation Systems
ERS	European Research Satellite
ESA	European Space Agency
GCIP	GEWEX Continental Scale International Project
GCM	General Circulation Model
GEWEX	Global Energy and Water cycle Experiment
HAPEX	Hydrological and Atmospheric Pilot Experiments
HEIFE	HEIhe river basin Field Experiment on the Atmosphere-Land surface Interaction
ECMWF	European Centre for Medium-range Weather Forecasting
HIRLAM	High Resolution Local Area Model
IGBP	International Geosphere Biosphere Programme
IIACE	Instituto de Investigaciones Aplicadas en Ciencias Espaciales
JORNEX	Jornada Experiment
KNMI	Koninklijk Nederlands Meteorologisch Instituut
LIPAP	Lanzhou Institute of Plateau Atmospheric Physics
LSP	Land Surface Process
LTER	Long Term Ecological Research
MERIS	MEdium Resolution Imaging Spectrometer
MLSAM	Mid Latitude Summer Atmospheric standard Model
MODTRAN	Moderate Resolution Transmittance
MSAVI	Modified Soil Adjusted Vegetation Index
NDVI	Normalised Difference Vegetation Index
NLR	Nationaal Lucht- en Ruimtevaartlaboratorium
NWP	Numerical Weather Prediction
PBMR	Push-Broom Microwave Radiometer
PBL	Planetary Boundary Layer
PRISM	Processes Research by an Imaging Space Mission
RACMO	Regional Atmospheric Climate Model
RAMS	Regional Atmospheric Modelling System
REBEX	Radiobrightness Energy Balance Experiment
RESMEDES	Remote Sensing of Mediterranean Desertification and Environmental Stability
SASSSIS	Spatial and Spectral Scales of Spaceborne Imaging Spectro-radiometers
SEBAL	Surface Energy Balance Algorithm for Land
SEBI	Surface Energy Balance Index
SSEBI	Simplified Surface Energy Balance Index
SGP97	Southern Great Plains 1997 hydrology experiment

SVAT	Soil Vegetation Atmosphere Transfer
TIMS	Thermal Infrared Multispectral Scanner
TIR	Thermal Infrared
TOA	Top Of Atmosphere
WAUMET	Wageningen Agricultural University, Department of Meteorology

The User Support Programme 1996-2005 (USP-2) is implemented under the responsibility of the Netherlands Remote Sensing Board (BCRS) and the Space Research Organization of The Netherlands (SRON).

The objectives of the USP-2 are: to support Dutch users of information from future European earth observation systems in the development of applications for operational and scientific use; to develop the required national infrastructure and to support users in developing countries with applications for the purpose of sustainable development, in connection with activities carried out by ESA and EUMETSAT.

The USP-2 is financed from the national space budget. During the period 1996-2000 the USP-2 element under the responsibility of the BCRS is executed in connection with the National Remote Sensing Programme 1996-2000.

Publication of:

Netherlands Remote Sensing Board (BCRS)
Programme Bureau
Rijkswaterstaat Survey Department

P.O. Box 5023
2600 GA Delft
The Netherlands
Tel.: +31 (15) 269 11 11
Fax: +31 (15) 261 89 62
E-mail: p.b.bcrs@mdi.rws.minvenw.nl
BCRS homepage: http://www.minvenw.nl/rws/mdi/bcrs